Title
Seasonal and interannual oxygen variability on the Washington and Oregon continental shelves

Journal
Journal of Geophysical Research C: Oceans, 120(2)

ISSN
2169-9275

Authors
Siedlecki, SA
Banas, NS
Davis, KA
et al.

Publication Date
2014

DOI
10.1002/2014JC010254

Peer reviewed

AGU PUBLICATIONS

JGR

Journal of Geophysical Research: Oceans

RESEARCH ARTICLE

10.1002/2014JC010254

Key Points:
- Oxygen model presented for the coastal ocean of the North American Pacific Northwest
- Respiration primarily controls seasonal oxygen loss on the shelf
- Spatial variability of respiration controls spatial variability of hypoxia

Correspondence to:
S. A. Siedlecki,
siedlesa@uw.edu

Citation:
Siedlecki, S. A., N. S. Banas, K. A. Davis, S. Giddings, B. M. Hickey, P. MacCready, T. Connolly, and S. Geier (2015), Seasonal and interannual oxygen variability on the Washington and Oregon continental shelves, *J. Geophys. Res. Oceans*, *120*, doi:10.1002/2014JC010254.

Received 18 JUN 2014
Accepted 27 NOV 2014
Accepted article online 8 DEC 2014

Seasonal and interannual oxygen variability on the Washington and Oregon continental shelves

S. A. Siedlecki[1], N. S. Banas[1], K. A. Davis[2], S. Giddings[3], B. M. Hickey[4], P. MacCready[4], T. Connolly[5], and S. Geier[4]

[1]Joint Institute for the Study of the Atmosphere and Ocean, University of Washington, Seattle, Washington, USA, [2]Department of Civil and Environmental Engineering, University of California, Irvine, Irvine, California, USA, [3]Scripps Institution of Oceanography, University of California, San Diego, La Jolla, CA, [4]School of Oceanography, University of Washington, Seattle, Washington, USA, [5]Woods Hole Oceanographic Institution, Woods Hole, Massachusetts, USA

Abstract The coastal waters of the northern portion of the California Current System experience a seasonal decline in oxygen concentrations and hypoxia over the summer upwelling season that results in negative impacts on habitat for many organisms. Using a regional model extending from 43°N to 50°N, with an oxygen component developed in this study, drivers of seasonal and regional oxygen variability are identified. The model includes two pools of detritus, which was an essential addition in order to achieve good agreement with the observations. The model was validated using an extensive array of hydrographic and moored observations. The model captures the observed seasonal decline as well as spatial trends in bottom oxygen. Spatially, three regions of high respiration are identified as locations where hypoxia develops each modeled year. Two of the regions are previously identified recirculation regions. The third region is off of the Washington coast. Sediment oxygen demand causes the region on the Washington coast to be susceptible to hypoxia and is correlated to the broad area of shallow shelf (<60 m) in the region. Respiration and circulation-driven divergence contribute similar (60, 40%, respectively) amounts to the integrated oxygen budget on the Washington coast while respiration dominates the Oregon coast. Divergence, or circulation, contributes to the oxygen dynamics on the shelf in two ways: first, through the generation of retention features, and second, by determining variability.

1. Introduction

The coastal ocean of Washington, British Columbia, and Oregon is an eastern boundary upwelling region that experiences a seasonal decline in oxygen on the shelf over the course of the upwelling season (usually May–October) [*Huyer et al*., 1979; *Landry et al*., 1989]. Oxygen levels often decline low enough to experience hypoxia (<1.4 mL/L, or <2 mg/L) [*Chan et al*., 2008; *Connolly et al*., 2010; *Crawford and Peña*, 2013; *Adams et al*., 2013; *Peterson et al*., 2013]. Upwelling regions, in general, frequently experience hypoxia and the associated negative impacts on the habitat for hypoxia-intolerant taxa of invertebrates and fish. For example, hypoxia has been linked to mass mortality events of these species off the coast of Oregon [*Grantham et al*., 2004; *Chan et al*., 2008]. Hypoxic zones are expected to expand with climate change, which will likely lead to a decrease in biodiversity in the affected habitats [*Levin et al*., 2009]. Some observational studies have found local respiration of organic matter to be an important driver of local oxygen dynamics in the northern portion of the California Current System [*Hales et al*., 2006; *Connolly et al*., 2010; *Adams et al*., 2013; *Crawford and Peña*, 2013]; while other studies [*Grantham et al*., 2004] found that the transport processes determined the observed oxygen levels. Understanding the processes that govern the seasonal decline of oxygen on the shelf is crucial to understanding how these systems will respond to future climatic forcing.

The coastal ocean off Oregon and Washington is subject to seasonal variations in wind stress. The mean winds shift in the spring from the winter downwelling-favorable southerly winds, to northerly, upwelling-favorable winds in summer [*Hickey*, 1979]. Deep, nutrient-rich, low-oxygen offshore water is upwelled onto the shelf and is transported to the euphotic zone where it fuels the highest productivity on the west coast of the U.S. [*Ware and Thomson*, 2005; *Hickey and Banas*, 2008]. The northern portion of the California Current System experiences significantly weaker upwelling winds than regions farther south, but *Hickey and Banas* [2008] attribute the high production of the British Columbia and Washington shelves to local freshwater

influences, wide shelves, and the presence of canyons, which draw water up onto the shelf from deeper depths than regions without canyons [*Hickey*, 1989, 1998; *Allen et al*., 2001; *Connolly and Hickey*, 2014; *Alford and MacCready*, 2014]. Recent work using the model described here emphasizes the importance of both the canyon and freshwater in the strong exchange flow that they drive through the Strait of Juan de Fuca [*Davis et al.*, 2014]. These high levels of primary production support standing stocks of particulate organic carbon (POC) in excess of 50 μmol kg^{-1} in British Columbia [*Ianson et al*., 2003] and 100 μmol kg^{-1} in Oregon [*Hales et al*., 2006], which includes phytoplankton and zooplankton biomass, as well as detrital carbon. While the high primary production produces oxygen at the surface, the POC sinks and respires into water already low in oxygen, driving the system toward hypoxia. Of the biological processes that influence oxygen concentrations in the coastal ocean, respiration of organic matter remains the most poorly understood. While respiration rates have been constrained by laboratory experiments and in the open ocean [*Dunne et al*., 1997; *Groussart and Ploug*, 2001], organic matter respiration on the shelf and slope is difficult to observe in the water column directly. Previous studies have used time series of oxygen concentration as a way to infer the contribution of respiration to the oxygen budget on the Washington-Oregon shelf [*Hales et al*., 2006; *Connolly et al*., 2010], or incubation experiments to quantify water column respiration [*Adams et al*., 2013]. In this paper, a high-resolution model of the region is used to determine the relative roles of divergence and local respiration of organic matter to seasonal oxygen decline on the shelf. In our model calculations, we find that respiration is responsible for 50–60% of the seasonal decline of oxygen on the Washington and Oregon shelves. Local retentive circulation processes determine the spatial patterns of respiration, which control the spatial distribution of hypoxia on the shelf.

1.1. Regional Circulation

The west coast of North America is an eastern boundary upwelling region, the California Current System (CCS) [*Hickey*, 1979]. In the spring and summer, seasonal northerly winds drive a coastal upwelling circulation characterized by regional equatorward flow over the shelf and upper slope, and a poleward undercurrent, the California Undercurrent, over the slope below the shelf break [*Hickey*, 1979, 1998]. In the northern CCS, freshwater and canyons become more important to cross-shelf exchange, and the shelf generally broadens [*Hickey and Banas*, 2008; *Allen and de Madron*, 2009]. Oceanic source waters for the water upwelled onto the shelves of Oregon, Washington, and British Columbia include the North Pacific Current and the California Current from the north, and, from the south, the California Undercurrent [*Hickey*, 1979].

Each of these currents has its own seasonal progression [*Hickey*, 1979; *Huyer et al*., 1979; *Hickey*, 1989; *Thomson and Krassovski*, 2010]. Over the slope of Washington, Oregon, and British Columbia, the spring transition to the upwelling season coincides with the onset of predominantly equatorward flow and a greatly reduced or sometimes absent California Undercurrent. The subsurface core of the poleward California Undercurrent shoals over the course of the upwelling season, occasionally surfacing as it travels north [*Pierce et al*., 2000]. When the upwelling season ends in the fall, the entire upper water column over the slope transitions to surface-intensified poleward flow, known as the Davidson Current.

The California Undercurrent water is salty, nutrient rich, and oxygen poor [*Hickey*, 1979; *Lynn and Simpson*, 1987]. It originates in equatorial regions and accumulates respired organic material as it travels north in subsurface layers. In contrast, the California Current travels equatorward in the upper $\sim$200 m of the water column, is highly oxygenated, but has a highly variable nutrient content. The nutrient content of the California Current varies in part due to the origin of this water, e.g., whether it originates in the subtropical North Pacific or subarctic Alaskan Gyres. The source water for the California Current has been implicated for driving hypoxic events on the Oregon shelf in the past [*Grantham et al*., 2004].

The seasonal trend in the slope water circulation of the region may result in a seasonal trend in the source water chemistry. As the poleward undercurrent shoals over the course of the upwelling season, it carries the oxygen-poor, nutrient-rich equatorial source waters with it [*Huyer et al*., 1979; *Huyer*, 1983; *Hickey*, 1979; *Hill et al*., 1998; *Pelland et al.*, 2013]. Studies suggest that the undercurrent contributes significantly (40–50%) to the composition of shelf water and upwelling source waters for the region [*MacFadyen et al*., 2008], carrying Pacific Equatorial Water ($\sim$20–40%) into the region [*Thomson and Krassovski*, 2010; *Meinvielle and Johnson*, 2013]. This has led to the hypothesis that the seasonal decline observed in oxygen on the shelf could be due to an increased contribution of undercurrent water over the course of the upwelling season.

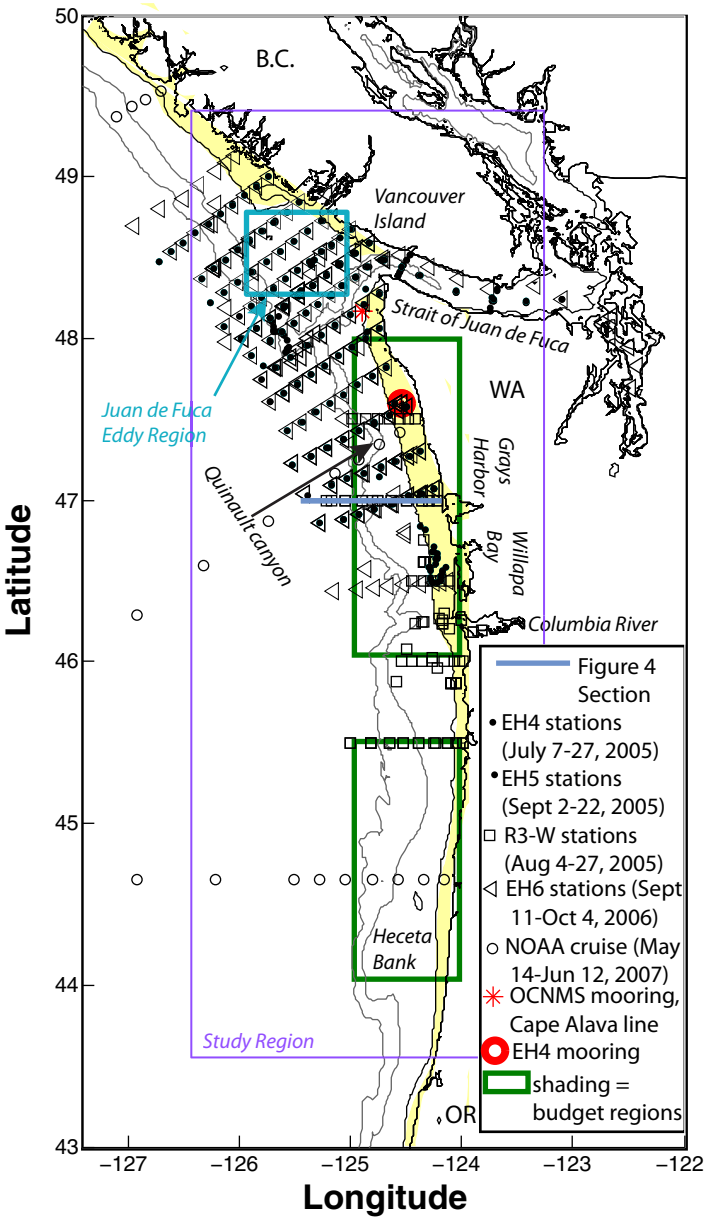

Figure 1. Model domain with locations of oxygen observations used to validate the model. The green outlined regions identify where budgets were calculated. Contours include the 60, 200, and 500 m isobaths. The region shallower than 60 m on the outer coast is shaded in yellow. The study region is outlined in purple to highlight the region focused on here, sufficiently away from the boundaries to avoid potential boundary issues.

In this study, a high-resolution model of oxygen cycling on the Washington and Oregon shelves is used to understand the relative contribution of physical processes and POC dynamics to the observed seasonal oxygen decline on the shelf over a period of 3 years (2005–2007). The modeling is done using the Regional Ocean Modeling System (ROMS), and the circulation model setup and validation are described in *Giddings et al.* [2014]. Oxygen is coupled to the biogeochemical model described by *Banas et al.* [2009a] and *Davis et al.* [2014] and validated here against observational data sets from 2005 to 2007 detailed in Figure 1. Oxygen budgets for the Washington and Oregon shelves are presented for the three modeled years. In section 2, the methods are outlined, including a description of the oxygen model. Section 3 summarizes the model simulations as well as model validation (sections 3.1 and 3.2). In section 4, controls over spatial variability in respiration are discussed. Finally, section 5 summarizes the results. We find that spatial and temporal patterns of oxygen are primarily controlled by local respiration on the shelf in this upwelling system.

2. Methods

2.1. Physical Model Setup

As part of the NOAA/NSF Pacific Northwest Toxins (PNWTOX) project, the Regional Ocean Modeling System (ROMS) [*Shchepetkin and McWilliams* 2005], a free-surface, hydrostatic, primitive equation model used extensively in coastal systems, was configured for the Washington and Oregon coasts (the "Cascadia" model) as described in detail by *Giddings et al.* [2014]. Surface forcing and boundary conditions for the realistic Cascadia simulations are specified as described in *Giddings et al.* [2014]. The domain extends from 43°N to 50°N, as shown in Figure 1, with a horizontal resolution on the shelf of 1.5 km and 40 vertical levels including the inland waters of the Salish Sea, a network of coastal waterways between British Columbia and the northwestern tip of the U.S. The Global Navy Coastal Ocean Model (GNCOM) is used for the open boundary and initial conditions [*Barron et al.*, 2006], and meterological forcing from the MM5 regional forecast model [*Mass et al.*, 2003] is applied. The model includes 16 rivers forced with daily river discharge and temperature data from U.S. Geological Survey (USGS) gauging stations and an Environment Canada gauging station for the Fraser River, as well as tides.

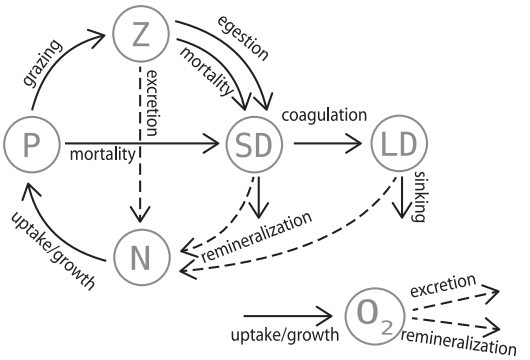

Figure 2. Cartoon of the biogeochemical model depicting the interaction of the reservoirs of Nutrients (N), Phytoplankton (P), Microzooplankton (Z), Small Detritus (SD), Large Detritus (LD), and Oxygen (O_2) in the model. Local observations were used to constrain the rates. Respiration rates were taken from *Dunne et al.* [1997] and *Groussart and Ploug* [2001]. Benthic flux parameterization was based on local historic benthic oxygen consumption data described in section 2 [*Hartnett and Devol*, 2003]. More information about the ecosystem model can be found in *Davis et al.* [2014].

GNCOM supplies the physical water properties (temperature and salinity) entering the domain at the open southern and western boundaries. Initial conditions for nutrients and oxygen were determined from empirical relationships with salinity using observations from *Connolly et al.* [2010]. Chemical and biological tracers are forced to obey a zero horizontal gradient on the open ocean boundaries. Thus, we assume that simulated values in the model domain are a reasonable estimate for what they would be outside the domain. For each of the 16 river point sources, constant values of oxygen (8 mL/L) and a climatological seasonal cycle for nutrients (see *Davis et al.*, 2014) are prescribed. An additional set of passive dye tracers was added to help visualize the source waters for upwelling on the shelf.

2.2. Biogeochemical Model Setup

The biogeochemical model consists of a five-compartment nitrogen budget and a coupled budget for dissolved oxygen (Figure 2). The nitrogen budget is based on the model of *Banas et al.* [2009a], with reparameterization of phytoplankton growth and the addition of a second detrital compartment as described below and in *Davis et al.* [2014]. Planktonic nutrient cycling in the model is described in detail by *Davis et al.* [2014], along with additional evaluation of model performance.

State variables include phytoplankton (P), zooplankton (Z), dissolved nutrients (N), small detritus (SD), large detritus (LD), and oxygen (O_2) (Figure 2). A list of variables and parameter values is given in Table 1. The model is written in terms of reservoirs of nitrogen, and conversion to oxygen is made with the Redfield ratio (138:16) [*Sarmiento and Gruber*, 2006]. Since ammonia concentrations are generally low (<10 μM), they are combined with nitrate into a single N pool. The choice of the ratio 138:16 assumes that nitrogen is in the form of nitrate and so includes oxidation of ammonia [*Ward*, 2008; *Paulmier et al.*, 2009].

The time evolution of oxygen (O_2) is calculated following *Bianucci et al.* [2011], using a modification of the framework of *Fennel et al.* [2006] as implemented in ROMS v2.2 (see also schematic in Figure 2, and equations in the Appendix A). Definitions and units for all variables are given in Table 1:

$$\frac{\partial O_2}{\partial t} = [\mu_i(E,N)P - (1-\varepsilon)(1-f_{egest})I(P)Z - rSD - rLD]C_{ox} + advection + diff \quad (1)$$

$$\left.\frac{\partial O_2}{\partial t}\right|_{bottom} = \frac{C_{2ox}}{\Delta z}\left(w_{SD}\left.\frac{dSD}{dz}\right|_{z=bottom} + w_{LD}\left.\frac{dLD}{dz}\right|_{z=bottom}\right) \quad (2)$$

$$\left.\frac{\partial O_2}{\partial t}\right|_{surface} = \frac{V_{O2}}{\Delta z}\left(\left.[O_2]\right|_{z=surface} - [O_2]_{sat}\right) \quad (3)$$

where $V_{O2} = 0.31u^2\left(\frac{Sc}{660}\right)^{-0.5}$, u is the wind speed at the surface, Sc is the Schmidt number from *Wanninkhof* [1992], and $[O_2]_{sat}$ from the *Garcia and Gordon* [1992] formula. Oxygen is produced by phytoplankton (P) growth (μ_i), which is light (E) and nutrient limited (N) as described in *Davis et al.* (2014). The functional response of zooplankton (Z) ingestion (I) is based on in situ microzooplankton dilution experiments [*Banas et al.*, 2009a]. Zooplankton excretion and egestion as well as respiration of both large (LD) and small detritus (SD) each draw down oxygen. The functional response for zooplankton (Z) ingestion (I) is based on extensive local observations of community grazing rates from dilution experiments [*Olson et al.*, 2008; *Banas et al.*, 2009a] and is consistent with laboratory measurements of grazing by herbivorous dinoflagellates and

Table 1. Ecosystem Model Parameters

	Description	Value	Source
μ_0	Maximum instantaneous growth rate	1.7 day^{-1}	RISE/ECOHAB observations: dilution experiments, 2003–2005 (n = 101)
att_{sw}	Light attenuation by seawater	0.05–0.0065(S-32) m^{-1} (where S = salinity)	RISE observations: PAR data from CTD casts, 2004–2005 (n = 43)
att_P	Light attenuation by phytoplankton	0.03 m^{-1}	RISE observations: PAR data from CTD casts, 2004–2005 (n = 43)
α	Initial slope of the growth-light curve	0.07 $(W\ m^{-2})^{-1}\ d^{-1}$	RISE/ECOHAB observations: photosynthesis-irradiance curves from deck-board incubations, 2004–2006 (n = 55)
k_s	Half-saturation for nitrate uptake (Optimal Uptake Model)	0.1	RISE/ECOHAB observations: dilution experiments, 2003–2005 (n = 101)
M	Nongrazing phytoplankton mortality	0.1 day^{-1}	A priori
$Chl{:}N$	Chlorophyll-to-nitrogen ratio	2.5 mg Chl $(mmol\ N)^{-1}$	RISE observations: CTDs 2004–2005 (n = 121)
I_0	Maximum ingestion rate	4.8 day^{-1}	RISE/ECOHAB observations: dilution experiments near growth-grazing equilibrium (n = 9)
ξ	Zooplankton mortality	2.0 $day^{-1}\ (\mu M\ N)^{-1}$	RISE/ECOHAB observations: dilution experiments near growth-grazing equilibrium (n = 9)
K_s	Half saturation for ingestion	3 $\mu M\ N$	Lab studies: average for ~60 microzooplankton and mesozooplankton spp. [*Hansen et al*., 1997]
ε	Gross growth efficiency of zooplankton	0.3	Lab studies: average for ~60 microzooplankton and mesozooplankton spp. [*Hansen et al*., 1997]
f_{egest}	Fraction of losses egested	0.5	A priori
R	Remineralization rate	0.1 d^{-1}	Th-based flux measurements at HOT [*Dunne et al*., 1997]Roller tank experiments on diatoms [*Groussart and Ploug*, 2001]
w_{LD}	Sinking rate for large detritus	80 m d^{-1}	A priori
w_{SD}	Sinking rate for small detritus	8 m d^{-1}	A priori
χ	Loss of nitrate to the sediments	1.2 mmol $NO_3\ m^{-2}\ d^{-1}$	Observations from the Oregon coast of a constant loss to the sediments from 80 to 1000 m [*Hartnett and Devol*, 2003]
τ	Detrital coagulation rate	0.05 $(mmol\ N\ m^{-3})^{-1}\ d^{-1}$	A priori
C_{ox}	Redfield conversion from O_2:N	138:16	
$C2_{ox}$	Redfield conversion from O_2:N for sediments	108:16	106:16 is Redfield; however, because the primary flux of nitrogen from the sediments is reduced, we are accounting for oxidation of ammonia stoichiometrically

ciliates [*Hansen et al*., 1997]. Both observation-based and model-based methods [*Olson et al*., 2006; *Banas et al*., 2009a] have concluded that in our study region, as in a wide range of marine environments [*Calbet and Landry*, 2004], microzooplankton have a much larger grazing impact on the phytoplankton than copepods and other mesozooplankton. *Banas et al*. [2009a] describes the derivation of zooplankton ingestion and mortality rate parameters from local field data, and *Davis et al*. [2014] validates the model results against these data. Dissolved organic matter (DOM) was not considered as a state variable in the model because the respiration of semilabile dissolved organic material has been shown to contribute small amounts to oxygen budget on the coast during the upwelling season, and more in winter [*Bianucci et al*., 2011; *Ianson and Allen*, 2002].

The key differences between this model and that of *Bianucci et al*. [2011] are in the formulation of direct denitrification at low oxygen concentrations in the water column, the lack of a sediment component, and a redesign of the detrital dynamics of the *Banas et al*. [2009a] model. In low oxygen environments (<5 μM), when oxygen is depleted, anaerobic respiration degrades organic material by utilizing various redox reactions of which denitrification is one. Direct denitrification consumes nitrate directly as the oxidizing agent for degradation of organic matter, and has been shown to be important in the sediments of the Washington shelf [*Christensen et al*., 1987; *Devol*, 1991; *Devol and Christensen*, 1993; *Connolly et al*., 2010] as well as in other regions. Water column direct denitrification is thought to be important globally in the open ocean suboxic zone [*DeVries et al*., 2012], but has yet to be considered in the coastal ocean. The threshold oxygen level below which denitrification can take place in the water column has not been absolutely determined, but some authors suggest it falls between 2 and 10 μM, from field observations in the Oxygen Minimum Zone off of Peru [*Codispoti et al*., 2005; *Brewer et al*., 2014]. In our model, under exceedingly low oxygen levels, when the respiration of detritus demands more oxygen than is available in a model time step, respiration consumes nitrate in the water column instead of oxygen.

A separate sediment component, like the one described in *Bianucci et al*. [2011], was not included in the model formulation here. This simplification assumes that organic carbon is consumed rapidly in the surface sediment layer and that little to no burial of organic carbon occurs on the shelves in the region. In support

of this assumption, observations from the Washington outer shelf (deeper than 70 m) from *Hartnett and Devol* [2003] determined that 8% of the primary production reaches the seafloor, and only 10–20% of that is buried in the sediments. Organic carbon in the sediments is mainly found deeper than the 50 m isobath, and comprises a small fraction (1–2%) of the sediments on the shelf [*Archer and Devol*, 1992]. These observations for the North American Pacific Northwest region, and the lack of consensus on burial controls [*Hedges and Keil*, 1995; *Macdonald and Pedersen*, 1991], suggest that most of the organic carbon reaching the seafloor is mineralized by the benthos and so can be modeled accordingly.

The redesign of the detrital dynamics of the *Banas et al*. [2009a] model mainly involved the addition of a large detrital class, and the elimination of burial at the bed. The large and small detritus classes differ in both their production mechanism and sinking velocities. The large detritus is produced as a result of coagulation (0.05 mmol N m^{-3} d^{-1}) of the small detritus [*Lima and Doney*, 2004]. The large detritus sinks at a rate of 80 m d^{-1}, and respires at the same rate as the small detritus (0.1 day^{-1}) [*Dunne et al*., 1997; *Groussart and Ploug*, 2001]. While this sinking rate is higher than previous modeling efforts, it is well within the observed range for diatoms, which dominate the primary production of upwelling regions. Lab experiments and field programs show that sinking velocities of diatoms and their associated aggregates exhibit sinking velocities between 10 and 1000 m/d [*Iverson and Ploug*, 2013; *Iversen and Ploug*, 2010]. Aggregates likely form within the large blooms of the region, and have been shown to contribute significantly to the sinking flux of organic matter [*Jackson et al*., 2005; *Healey et al*., 2009; *Ianson et al*., 2012]. At the bed, all detritus respires and returns to the nutrient pool as in *Fennel et al*. [2006] using the stoichiometric ratio of O_2:N = 108:16 for coupled denitrification, slightly altered to account for the oxidation of ammonia back to nitrate (see equations (A1) in Appendix A and *Davis et al*. [2014]). Because we assume (following *Fennel et al*. [2006]) that the sinking flux out of the bottommost grid cell results in an immediate, corresponding influx of nutrients at the sediment-water interface and an oxygen loss to the sediments, this flux can also be equated to the sediment oxygen demand. Observations of the sediment oxygen demand on the Washington shelf [*Hartnett and Devol*, 2003] were therefore used to constrain the sinking velocity of the large detritus and the coagulation rate (Table 1), parameters which are often completely unconstrained in biogeochemical models. Additionally, a quasi-one-dimensional ROMS model (see next section) was used to test the impact of various detrital scenarios on nutrient profiles. The nutricline was better represented with two detrital pools, which ultimately results in better prediction of the depth of organic matter respiration.

2.3. Detrital Dynamics Sensitivity

The design of the detrital portion of the model was crucial to achieving good agreement between the modeled and observed oxygen concentrations. Several variations of the detrital model were tested and compared with data. The bottom boundary condition (reflective versus burial), inclusion of a second detrital pool, and sinking velocity were varied, while respiration rate and other model parameters were held constant. The goal of the tests was to achieve the same rate of change observed in the oxygen concentrations from the moored observations at EH4 (see Figure 1), a Washington shelf mooring in 32 m of water with sensors 1 m off the bottom [*Connolly et al*., 2010].

The bottom boundary condition was tested by comparing a case in which detritus was allowed detritus to sink out of the bottom, or be buried, to a case where detritus was instantaneously respired, or a reflective boundary condition. The case that allows burial on the shelf causes the modeled oxygen concentration in bottom waters to remain steady over the course of the upwelling season, unlike the observed trend. Only when detritus was not buried, but instead instantly respired, was the rate of change of oxygen similar to observations. This "reflective" boundary condition assumes a steady state in which the nutrient flux to the sediments is equivalent to the pore water nutrient flux back to the water column. This is a good assumption at steady state, and is consistent with the *Fennel et al*. [2006] model formulation. By allowing the nutrients to respire on the shelf and oxygen to decrease in response, the oxygen concentrations decrease on the shelf over the upwelling season in the model. However, the resulting modeled oxygen concentrations were biased too low, indicating excessive oxygen depletion on the shelf. Given a remineralization rate of 0.1 day^{-1} [*Groussart and Ploug*, 2001; *Wetz et al*., 2008], a detrital particle must sink faster than 20 m d^{-1} in order to respire deeper than the shelf break (200 m). By increasing the sinking velocity of a single particle detrital pool, detritus respires deeper than 200 m because it sinks faster, escaping the nutrient trapping on the shelf. However, the resulting modeled oxygen declines too quickly, and removes nutrients too quickly from the surface, thus negatively affecting primary production (not shown).

Through the addition of a second detrital class, the surface bloom remains unaffected, while some of the nutrients are allowed to escape nutrient trapping on the shelf. Nutrients did not experience a net trend on the shelf or elsewhere in the domain from year to year when the second detrital class was added. The nutricline was more realistically represented with the addition of the second detrital class, which ultimately produced better results for oxygen as well.

2.4. Model Experiment

Realistic hindcast simulations were run continuously for 2004–2007 as described by *Giddings et al*. [2014]. One year of simulation (2004) was required to ensure that the dye and biogeochemistry were spun-up to steady state. Steady state in the biogeochemistry is defined as the state where less than a 1% change in total nutrients occurs in the domain interannually. Thus, here we present results from 2005–2007 only.

Each simulated year experienced very different environmental forcing. For example, 2005 was characterized by a late onset for the upwelling season [*Kosro et al*., 2006]. In contrast, 2006 experienced prolonged and extensive upwelling with the most river discharge. 2007 is described as a moderate upwelling season with a record snowpack producing high discharge in the spring/early summer months. The implications of these very different environmental forcings will be discussed in section 4.

2.5. Budget Calculations

Oxygen budgets for the shaded regions depicted in Figure 1 were calculated from the model results using equation (1) and the diagnostic terms from ROMS. The diagnostic fluxes, both the advective and diffusive terms for the tracers as well as the biogeochemical model fluxes were averaged daily. Each diagnostic flux, representing terms in equation (1), was vertically integrated over 0–500 m, time averaged over the upwelling season as defined by the 8 day wind stress, and then spatially averaged over the regions outlined in Figure 1. The upwelling seasons for each year are defined in Table 2 and consistent with the spring and fall transition dates as determined by the cumulative upwelling index. The region in Oregon was cut off at 44°N to avoid model boundary effects, and thus that region mostly represents Heceta Bank (Table 2). Primary production is a source of oxygen from the production of organic matter as defined in equation (1). Respiration is the sum of the water column respiration of detritus, zooplankton egestion, and sediment oxygen demand, and is always a loss of oxygen. Air-sea exchange is the contribution to the budget of gas exchanges as defined in equation (3) and can be a source or a sink of oxygen. Divergence is defined as the sum of horizontal plus vertical advective and diffusive fluxes, and can be either a source or a sink of oxygen. When the divergence contribution is positive, two scenarios exist: either oxygenated water is imported into the region or low-oxygen water is exported out of the boxed region (or both, in different layers within the 0–500 m range of integration).

3. Results

3.1. Model Validation

Bottom water oxygen concentrations are lowest during the summer upwelling season [*Connolly et al*., 2010; *Pierce et al*., 2012; *Crawford and Peña*, 2013], and recent observations are mostly limited to this period. Consequently, the focus of the analysis here is on summer dynamics (2005–2007); however, it should be noted that the model was run continuously for four full seasonal cycles. Observations used for validation are shown in Figure 1 and span the entire upwelling season, capturing the beginning and end at certain locations. Validation results for oxygen, based on over 2264 CTD casts, and brief results for the physical and biological fields are presented here. More extensive analysis of modeled nitrogen and chlorophyll are presented in *Davis et al*. [2014] and modeled temperature, salinity, and velocity are presented in *Giddings et al*. [2014].

3.1.1. Physical Model Validation Summary

The physical model successfully reproduces the dominant features, such as coastal upwelling and Columbia River plume movement, and regional oceanography, such as coastal-trapped waves, with significant skill (Willmott Skill Score of >0.5, discussed further below) in 2005 on both event and seasonal time scales [*Giddings et al*., 2014]. The observations are extensive including locations marked on Figure 1 and additional locations indicated in *Giddings et al*. [2014, Figure 1]. Observations are more prevalent on the shelf and near

Table 2. Oxygen Budget for Washington and Oregon Boxed Regions Identified in Figure 1[a]

Washington shelf	Budget Term	Averaged Over 2005 Upwelling Season (DOY 150–270)	Std Dev (2005)	Averaged Over 2006 Upwelling Season (DOY 493–670)	Std Dev (2006)	Averaged Over 2007 Upwelling Season (DOY 860–1000)	Std Dev (2007)	Average (2005–2007)	Interannual Variability (Std Dev)	Percent of (Prod-dO/dt)
	Primary production	118	40	123	48	127	35	123	5	
	Air-sea gas exchange	−6	23	3	35	−9	36	−4	6	−3%
	Divergence	−77	110	−50	140	−50	127	−59	16	−38%
	Total Respiration	−87	26	−94	25	−98	15	−93	6	−60%
	Consumption in Water Column	−64	20	−69	18	−73	11	−69	5	
	Sediment Oxygen Demand	−23	7	−25	8	−26	6	−25	2	
	Temporal Change (dO/dt)	−52	96	−18	128	−30	112	−33	17	

Oregon shelf	Budget Term	Averaged Over 2005 Upwelling Season	Std Dev (2005)	Averaged Over 2006 Upwelling Season	Std Dev (2006)	Averaged Over 2007 Upwelling Season	Std Dev (2007)	Average (2005–2007)	Interannual Variability (Std Dev)	Percent of (Prod-dO/dt)	Heceta Bank (44–45N,HB) Avg Only (2005–2007)	HB Interannual Variability (Std Dev)
	Primary production	72	18	91	26	94	25	86	12		88	13
	Air-sea gas exchange	−33	16	−33	28	−43	29	−36	6	−31%	−39	5
	Divergence	5	103	3	98	−10	61	−1	8	−1%	0	9
	Total Respiration	−67	11	−85	18	−90	21	−81	12	−69%	−83	12
	Consumption in Water Column	−60	11	−78	16	−83	19	−74	12		−74	11
	Sediment Oxygen Demand	−7	1	−7	2	−8	2	−7	1		−9	1
	Temporal Change (dO/dt)	−23	103	−24	99	−49	70	−32	15		−32	13
	Summer Average 8 day Wind Stress	7.3		7.2		2.4						
	Winter Average 8 day Wind Stress	−25.5		−22.2		−23.2						

[a]The fluxes were integrated over the top 500 m, and then averaged over the upwelling season, as defined by the 8 day wind stress. The upwelling season for each year is shaded in gray on Figure 13. The time series for each of these fluxes is plotted in Figure 13. In addition, the standard deviation for each upwelling season is also reported. The table includes the average over all 3 years and the standard deviation, or interannual variability, of all the fluxes. Finally, the average wind stress over the summer upwelling and winter seasons is also reported.

the surface during the late spring and summer months (May–October), resulting in our greatest confidence in these regions and at these times. Geographically, the observations are more concentrated on the Washington and British Columbian coasts. The observations include in situ hydrodynamic observations, satellite data, and glider data including time series. The model currents, salinity, and temperature are validated using an extensive array of physical observations including in situ hydrodynamic observations (time series and transects), satellite data, and glider data [see *Giddings et al*., 2014, Figure 1]. Mooring records were provided from the Ecology and Oceanography of Harmful Algal Blooms—Pacific NorthWest (ECOHAB-PNW) and River Influences on Shelf Ecosystems (RISE) projects (May–September 2004–2007) as well as the Fisheries and Ocean Canada, Institute of Ocean Sciences (IOS) (year round). Moorings had acoustic Doppler current profilers (ADCPs) and conductivity, temperature, depth sensors (CTDs) or temperature sensors at varying depths. Tidal and subtidal sea surface height was validated using NOAA tide gauges (http://tidesandcurrents.noaa.gov/). Finally, CTD casts throughout the domain were used to test the vertical distribution of temperature and salinity. These included casts from the spatially comprehensive ECOHAB-PNW [*MacFadyen et al*., 2008] and RISE [*Hickey et al*., 2010] projects as well as the Puget Sound Regional Synthesis Model (PRISM), Washington State Department of Ecology, the Joint Effort to Monitor the Strait (JEMS), and IOS (Figure 1) totaling over 7000 CTD casts and 10 moorings from 2004 to 2007. Note that casts span the entire year, although the majority of the offshore casts were taken during the upwelling season. Figure 3 shows the subtidal and mean velocity, salinity, and temperature comparisons at a mooring (EH4). All subtidal time series are computed with a Godin low-pass filter [*Emery and Thomson*, 2004]. The model velocities achieve better skill in the alongshore direction than the cross-stream direction.

In general, the model represents the circulation on the shelf better than beyond the shelf break, but the model has significant skill at all compared depths (down to 500 m) [*Giddings et al*., 2014]. The model reproduces the strengthening and shoaling of the California Undercurrent (Figure 4) [*Giddings et al*., 2014]. Figure 4 includes a cross section at 47°N during the spring and again in late summer during the peak California Undercurrent presence in 2005. The California Undercurrent is seen in Figure 4 as a poleward velocity core centered near the shelf break. In addition, the California Undercurrent can be identified using the a passive

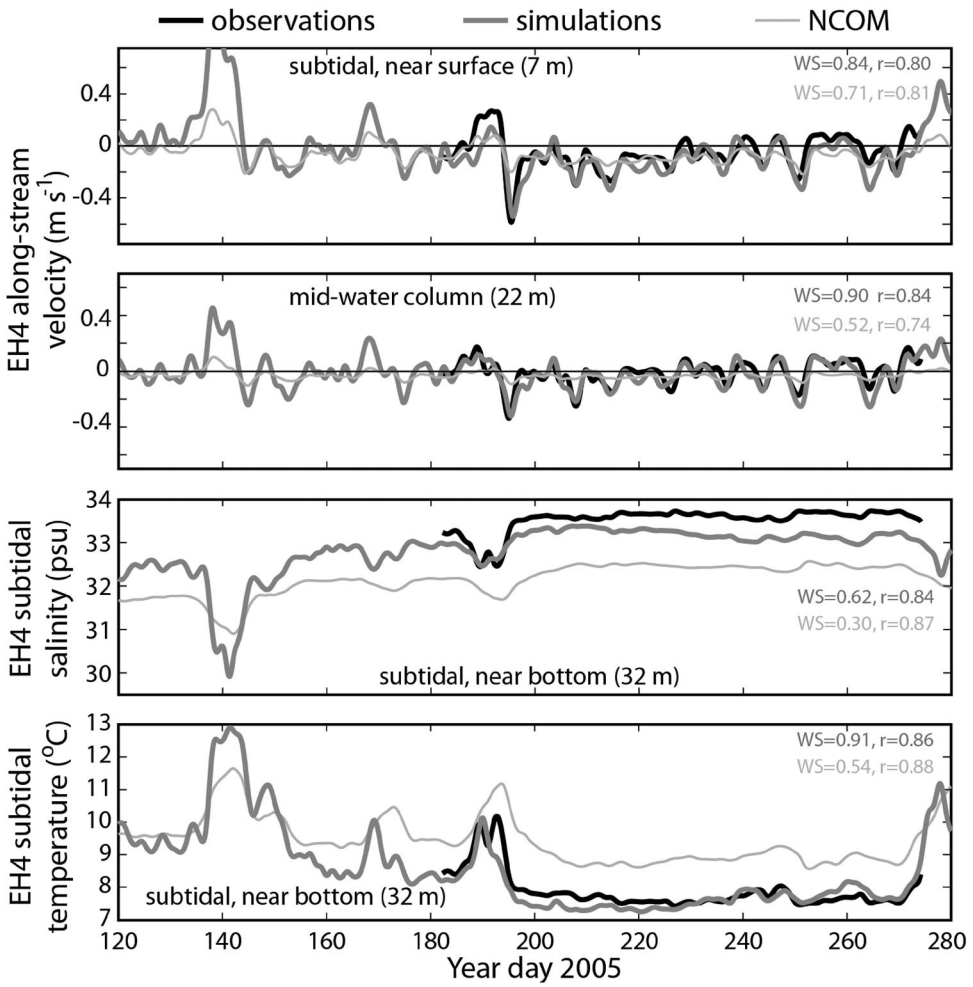

Figure 3. Modeled fields for summer of 2005. Subtidal time series near the water surface and mid-water column (22 m) along-stream (top) velocity, (middle) salinity, and (bottom) temperature at EH4, an ECOHAB-PNW mooring, in 32 m of water. Observations are in black, model results are in gray, and NCOM results are in thin light gray. Willmott skill scores (*WS*) and correlation coefficient (r) are included on the panels for the near-surface subtidal time series. For more information about the model circulation, see *Giddings et al*. [2014].

dye tracer in our model entering at the southern boundary, or in the nitrate and oxygen fields, as high nitrate, low oxygen, and high dye concentrations.

3.1.2. Biogeochemical Model Validation Summary

To quantify the overall correspondence between the observations and modeled oxygen fields, target diagrams [*Jolliff et al*., 2009] were made from profile observations and colocated model profiles (locations shown in Figure 1) in order to provide a summary of the pattern statistics and model biases (Figure 5). The distance from the origin in Figure 5 is proportional to the total Root Mean Squared Difference (RMSD). Figure 5 informs whether the model's standard deviation is larger ($X > 0$) or smaller ($X < 0$) than the standard deviation of the observations, in addition, to providing information about the positive ($Y > 0$) or negative ($Y < 0$) bias. Modeled oxygen is biased low (<0.5 mL L^{-1}) and the standard deviation in the oxygen fields is larger than the observed standard deviation. Still, modeled oxygen fields mostly fall within values of 1 of the RMSD and Bias, each normalized by the standard deviation of the observations. This result indicates a better than average modeling efficiency metric (MEF) [*Stow et al*., 2009], and that the observations and colocated modeled points are positively correlated [*Jolliff et al*., 2009]. Consistent with the oxygen results, shown in Figure 5, modeled nitrate is biased high for observed nitrate values less than 10 μM, typically near the surface, as pointed out in *Davis et al.* [2014]. The model also has a slight (<5 μM) bias high at depth consistent with the fresh bias in salinity inherited from our NCOM boundary conditions [*Davis et al*., 2014].

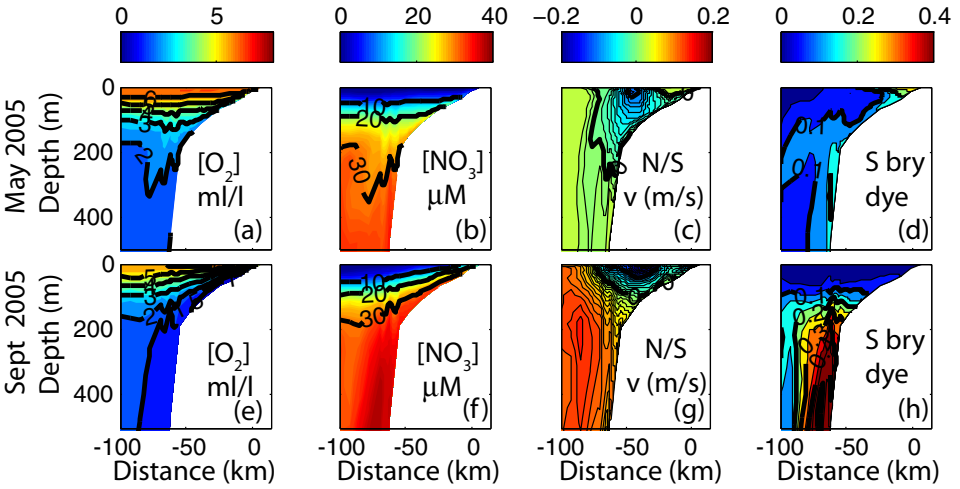

Figure 4. Modeled fields for summer of 2005. Cross sections along 47°N (top row) averaged over the month of May and (bottom row) averaged over the month of September. The model reproduces the observed seasonal cycle of the slope circulation with a minimal undercurrent in the spring and a strong undercurrent in the late summer. (a) Oxygen in mL L^{-1}, (b) nitrate in Mm, (c) alongshore velocity in m s^{-1} (positive poleward), (d) southern boundary dye concentration. The undercurrent can be identified in the model by the poleward (positive) flow, high concentration of southern boundary dye (S bry dye), high nitrate, low oxygen water. For more information about the model circulation, see *Giddings et al.* [2014].

Modeled standard deviation in the nitrate fields is smaller than the observed standard deviation over the same space and time (not shown). Further validation of the model fields are presented below in the form of maps, cross sections, and time series comparisons.

3.1.3. Time Series and Mooring Comparisons

Oxygen on the inner shelf experiences a dramatic seasonal variation and seasonal decline during the summer to early fall. Event-scale fluctuations are superimposed on top of this seasonal trend. Oxygen and temperature time series from moorings on the northern Washington shelf (EH4 and CA065, shown in Figure 1) are compared to modeled oxygen and temperature (Figure 6). To assess model skill in the time series comparisons, the Willmott Skill Score (*WSS*) [*Willmott*, 1982] is used:

$$WSS = 1 - \frac{\frac{1}{N}\sum_{i=1}^{i=N}(m_i - o_i)^2}{\frac{1}{N}\sum_{i=1}^{i=N}(|m_i - \bar{o}| + |o_i - \bar{o}|)^2} = 1 - \frac{MSE}{\frac{1}{N}\sum_{i=1}^{i=N}(|m_i - \bar{o}| + |o_i - \bar{o}|)^2} \quad (4)$$

where o_i is an observation, m_i is the corresponding model value, there are N paired modeled/observed values, and *MSE* is the mean square error. The *WSS* is an index of agreement between the observed and modeled values, with a value of 1 indicating perfect agreement and a value of 0 indicating no agreement, and incorporates both the mean bias between modeled and observed values and the variability about that mean bias [*Willmott*, 1982].

At EH4 on the Washington shelf (see location in Figure 1), the model reproduces the observed seasonal oxygen decline in 2005 despite a poor correlation with the observations on the event scale ($R^2 = 0.002$, $WSS = 0.33$; Figure 6a). The model predicts the onset of hypoxia (<1.4 mL/L) within 2 days of the observations at EH4 in 2005, but ends the season with higher than observed concentrations. *Connolly et al.* [2010] show that the observed event-scale variability is associated with along-shelf advection of a low-oxygen patch rather than upwelling and downwelling. Despite missing the event-scale variability, the model's performance in 2005 is representative in a seasonal sense (Figure 5). The model also captures the seasonal decline in oxygen on the inner Washington shelf in 2006 ($R^2 = 0.53$, $WSS = 0.81$), and 2007 ($R^2 = 0.68$, $WSS = 0.91$), as well as most of the event-scale variability (Figure 6). In 2006, the model predicts the onset of hypoxia 10 days prior to the observations at EH4. A warm, high-oxygen event near the end of September 2006 is the signature of a downwelling wind event. The upwelling season ends abruptly with the fall transition to warmer temperatures and higher oxygen in October of all 3 years. In 2007, the observational record continued through the end of the year, and the model captures the fall transition.

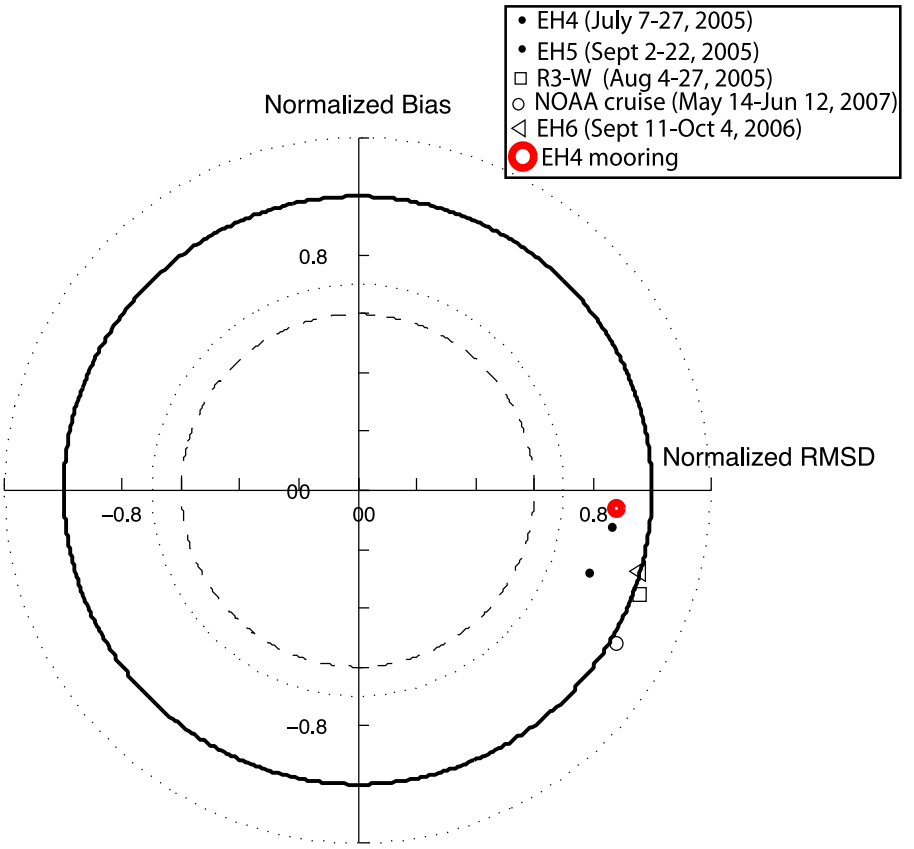

Figure 5. Target diagram for modeled oxygen from all years over the upwelling season. Each cruise sample location (EH4, EH5, EH6, R3W, and NOAA) as well as the mooring (EH4) is depicted as shown in Figure 1. The figure informs whether the model's standard deviation is larger ($X > 0$) or smaller ($X < 0$) than the standard deviation of the observations, in addition, to providing information about the positive ($Y > 0$) or negative ($Y < 0$) bias. Observations span <30 m down to 3000 m depth and consist of both CTD oxygen sensor data as well as bottle samples.

In contrast to EH4, time series from mooring CA065 at midshelf (depth = 65 m) in the Olympic National Marine Sanctuary off the Washington coast (~48°N, see Figure 1) show this location rarely experienced hypoxia in 2006–2007. The model has one brief hypoxic event in 2006 and another in 2007 (September of 2006 for 2 days, and August of 2007 for 4 days) that is earlier and not as severe as observed. Possible reasons for this region's generally normoxic (oxygen concentrations greater than hypoxic concentrations) conditions are discussed later.

3.2. Spatial Patterns in Oxygen Over the Upwelling Season

Spatial patterns of bottom oxygen show both mesoscale and regional variability (Figure 7). Patterns are similar to the observations, depicted as maps of bottom oxygen from two late summer CTD surveys [*Connolly et al.*, 2010] compared to modeled oxygen from the same time interval (Figure 7). In each case, the model field was averaged over the time interval of sampling observations, roughly 1 week. In 2005, both model and observations show that the region beneath the seasonal Juan de Fuca Eddy is hypoxic, while the adjacent shelves both north and south of the Juan de Fuca Eddy remain oxygenated. Further south on the Washington coast, offshore of Grays Harbor (46°N–47°N), hypoxia was observed and the model captures this pattern. In 2006, the modeled hypoxic region under the Juan de Fuca eddy extends farther onto the British Columbia shelf than the observed pattern. The area of lowest oxygen is again located offshore of Grays Harbor (46°N–47°N). The model does indicate a thin band of oxygenated water hugging the coast in that area, a region not sampled by the observations. Thus, although the modeled hypoxic regions do not overlap exactly with the observations, the general spatial patterns and gradients observed are reproduced in the model.

The seasonal progression in 2005 of low-oxygen water on the Washington shelf is illustrated with modeled and observed cross sections from the same location and time period (Figure 8). The observations illustrate

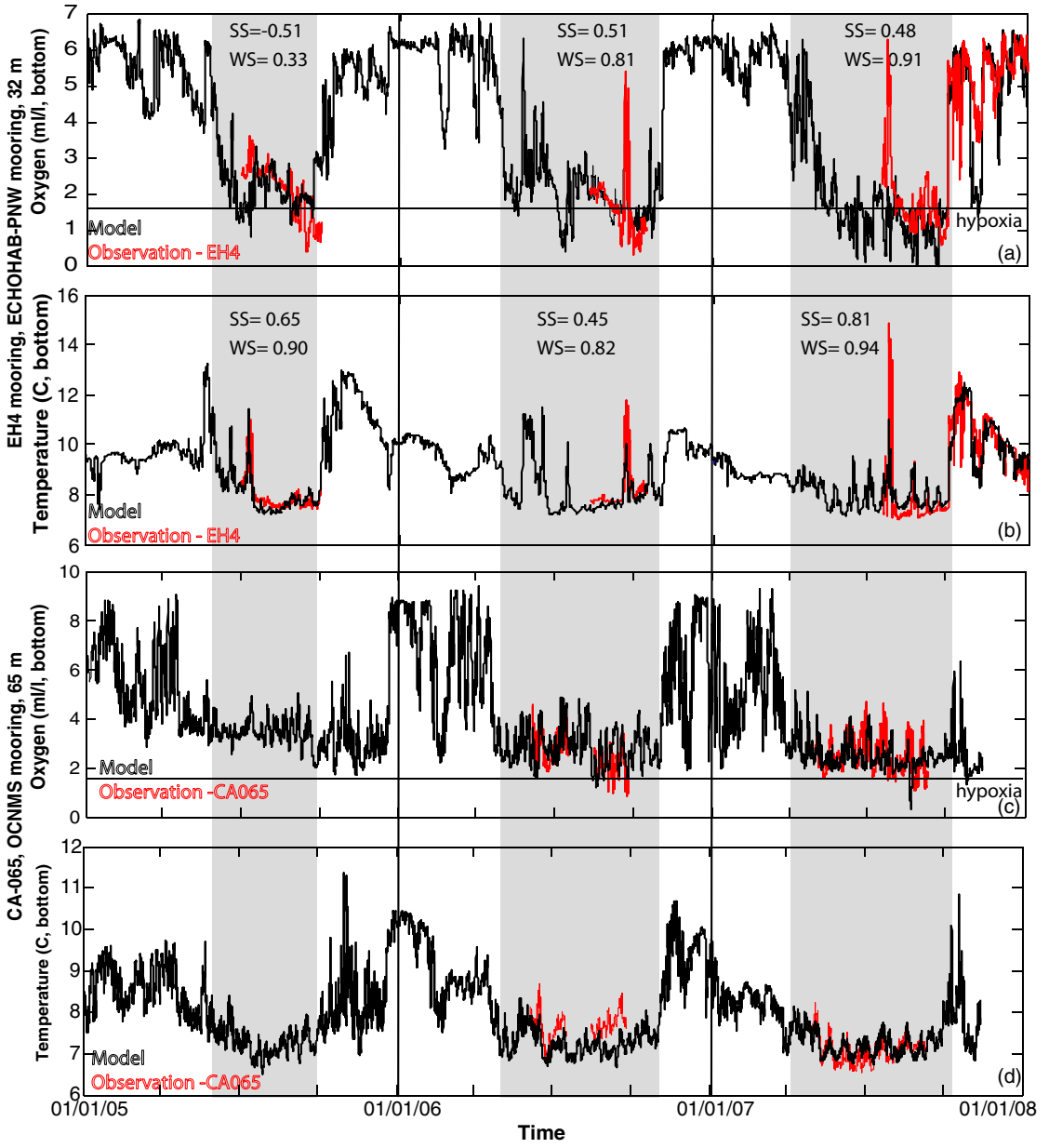

Figure 6. Time series from 2005 to 2007 of (a) bottom oxygen and (b) bottom temperature from the model (black) and observations at EH4 (red)—a mooring around 47.5°N in 32 m of water from *Connolly et al.* [2010], see Figure 1. Time series of (c) bottom oxygen and (d) bottom temperature from the model (black) and observations at CA065 (red)—a mooring from the Olympic Coast Marine Sanctuary around 48°N in 65 m of water for 2006–2007, see Figure 1. Upwelling seasons have been shaded by gray boxes. Units are mL $L^{-1}$and hypoxia (<1.4 mL L^{-1}) marked as a constant line on the oxygen panels. Both the Willmott Skill Score (WS) and the Skill Score (SS) are included on the plot for each observational period.

that low-oxygen water upwells onto the shelf in a thin layer along the bottom (Figure 8). Hypoxic water develops first in patches on the mid shelf (Figure 8e), expanding farther onto the shelf and extends higher into the water column over the course of the upwelling season (Figure 8p). The model reproduces the observed seasonal progression (Figure 8a versus Figure 8l). In the beginning of the upwelling season, high-oxygen (>3 mL/L) water dominates the water column on the inner shelf. By the end of the season, the low-oxygen (<2 mL/L) water dominates the water column, occupying more than 50% of the water column. Second, the model simulates the seasonal progression in the thickness of the highly oxygenated surface layer (>6 mL/L). The surface layer progresses from occupying more than the upper 50 m of the inner shelf in May to occupying less than 20 m by September in both the model (Figures 8a and 8l) and the observations (Figures 8e and 8p). The thinning of the surface oxygenated layer over the course of the upwelling season coincides with the thickening of the oxygen depleted bottom water.

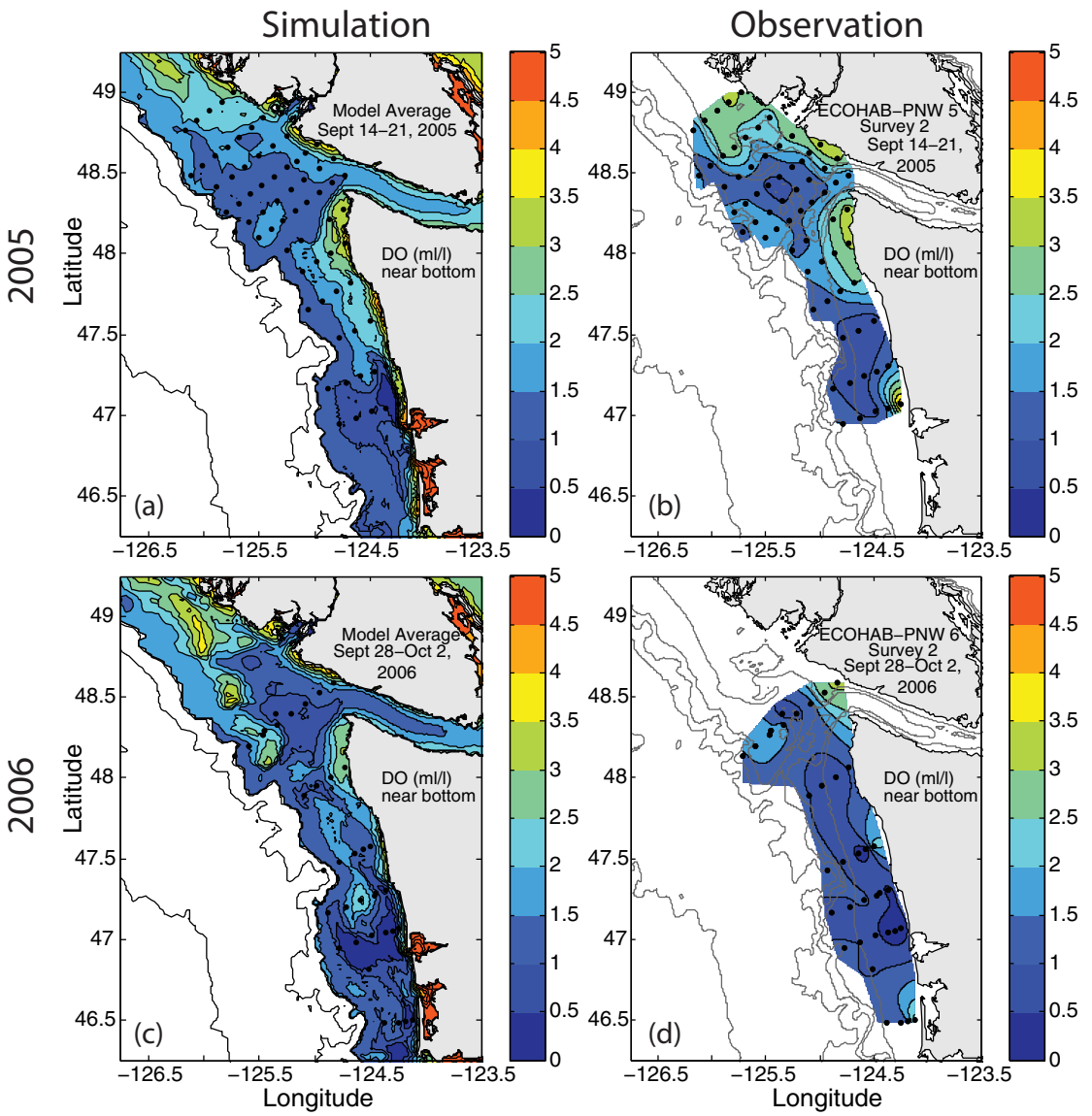

Figure 7. Maps of bottom oxygen from the model (a) and (c) and the observations (b) and (d) for the same time periods in 2005 and 2006. Model results are shown for the entire shelf region and thus are not subsampled to the observation locations. Observations made as part of the ECOHAB-PNW program and described by *Connolly et al.* [2010] are taken at the black dots and objectively contoured. Observations adapted from *Connolly et al.* [2010]. Units are mL L^{-1}.

3.3. Modeled Seasonal Oxygen Patterns in the North American Pacific Northwest

With confidence derived from comparison with the comprehensive Washington database, results are now extended to the entire North American Pacific Northwest. The seasonal progression of oxygen decline on the shelf in each of the 3 years is clearly evident in time-averaged maps of modeled bottom oxygen over much of the study region (Figure 9). While all 3 years experienced hypoxia on the shelves of Oregon and Washington, the spatial extent and onset shows significant interannual variation, e.g., the British Columbia shelf only experiences hypoxia in 2007. Hypoxic regions develop on the shelf in late summer of each upwelling season. Three regions persistently experience hypoxia in the model: the Washington shelf just north of Grays Harbor (46°N–47°N); the Juan de Fuca Eddy region; and Heceta Bank, Oregon (Figure 10).

The British Columbia shelf generally experiences the highest bottom oxygen concentrations. As shown by *Crawford and Peña* [2013], development of seasonal hypoxia only occurs in the region around the Juan de Fuca Eddy at the mouth of the Strait of Juan de Fuca, south of 49°N. On the coast of British Columbia in the model, the largest area of hypoxic shelf water occurs in late summer of 2007. The predominantly oxygenated subarctic North Pacific water to the north and the northward-flowing Vancouver Island Coastal Current

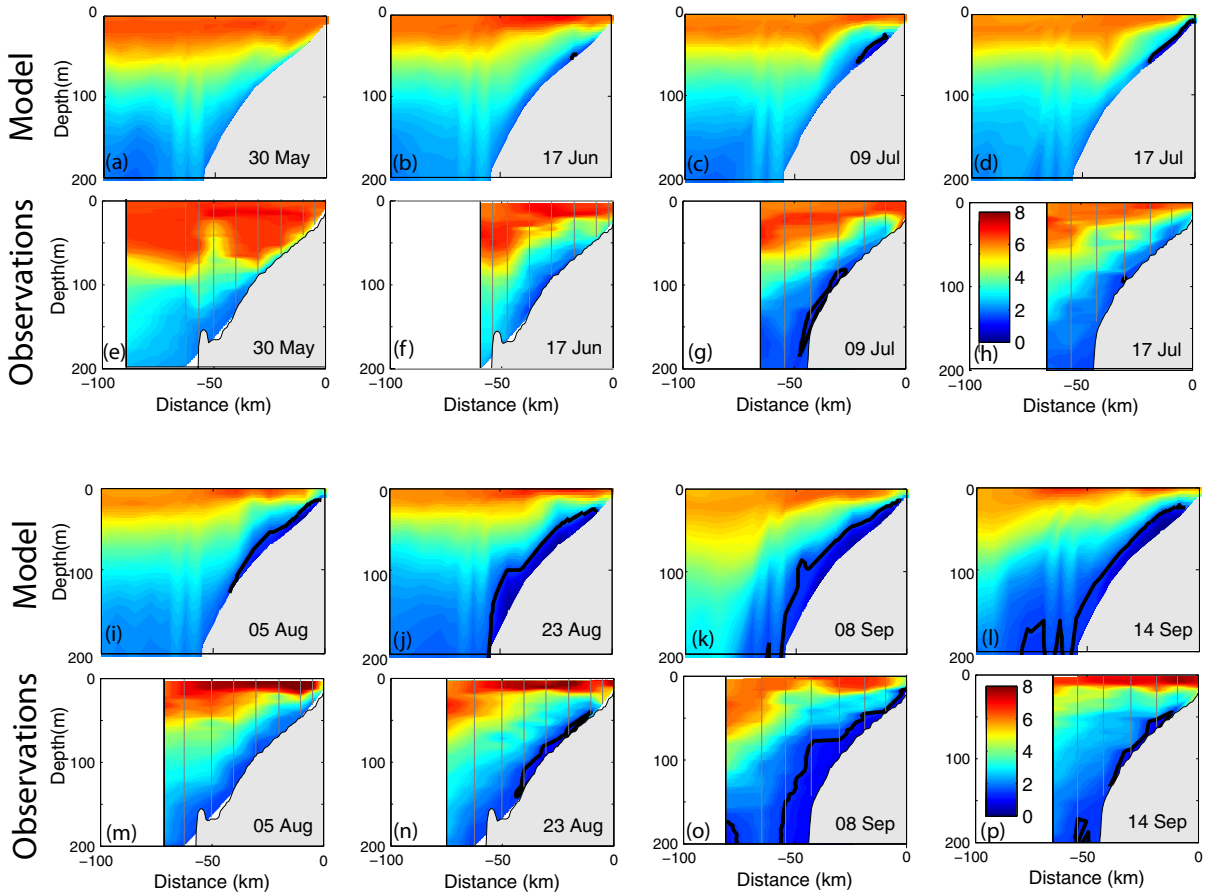

Figure 8. Cross sections of oxygen in the water column from (top) the model and (bottom) the observations for the same time periods in 2005. Observations made as part of the ECOHAB-PNW program and described by *Connolly et al*. [2010] along the vertical gray lines. Observations adapted from *Connolly et al*. [2010]. Units are mL/L and hypoxia (<1.4 mL/L) is outlined by the black contours.

(VICC) dominate the British Columbia coast, allowing the shelf to remain oxygenated [*Bianucci et al*., 2011]. The buoyancy-driven VICC is associated with downwelling isopycnals at the coast, which opposes wind-driven upwelling [*Hickey et al*., 1984]. This issue will be discussed further in section 4.1.

The shelf region offshore of Grays Harbor from north of the Columbia River mouth to south of Quinault canyon (~46°N–47°N) is the broadest section of shallow (<60 m) shelf off Washington and Oregon. Heceta Bank is the broadest shelf off Oregon (width ~40 km), similar in width to the widest regions of the Washington shelf (width ~50 km), but much deeper than the Washington shelf (117 m versus 75 m, on average). The relative importance of shelf width and depth to the oxygen demand will be discussed in section 4.1.

3.4. Modeled Spatial Patterns of Respiration in the Northern California Current

The regions that repeatedly experience the lowest oxygen concentrations on average in the modeled years correspond to regions of enhanced respiration, either in the water column or in the sediments (sediment oxygen demand) (Figure 10). While observations of respiration in the water column are rare, the range of respiration from the model (0.25–0.75 mmol O_2 m^{-3} d^{-1}, 0.006–0.017 mL L^{-1} d^{-1}) overlaps with the observed range discussed in *Adams et al*. [2013] (0.014–0.045 mL L^{-1} d^{-1}) based on observations from the Oregon shelf at 70 m during the upwelling season. In Figure 10, respiration was integrated over 200 m of the water column and averaged over the upwelling season (May–September) for each year. The Juan de Fuca Eddy region, the central Washington coast, and Heceta Bank are regional hot spots in the maps of total integrated respiration.

The Washington shelf experiences more sediment oxygen demand (Figure 10, second column) than the Oregon shelf. This spatial pattern is consistent with observations from two locations. *Hartnett and Devol* [2003] report sediment oxygen demand of 20 mmol O_2 m^{-2} d^{-1} on the Washington shelf at 80 m depth. On

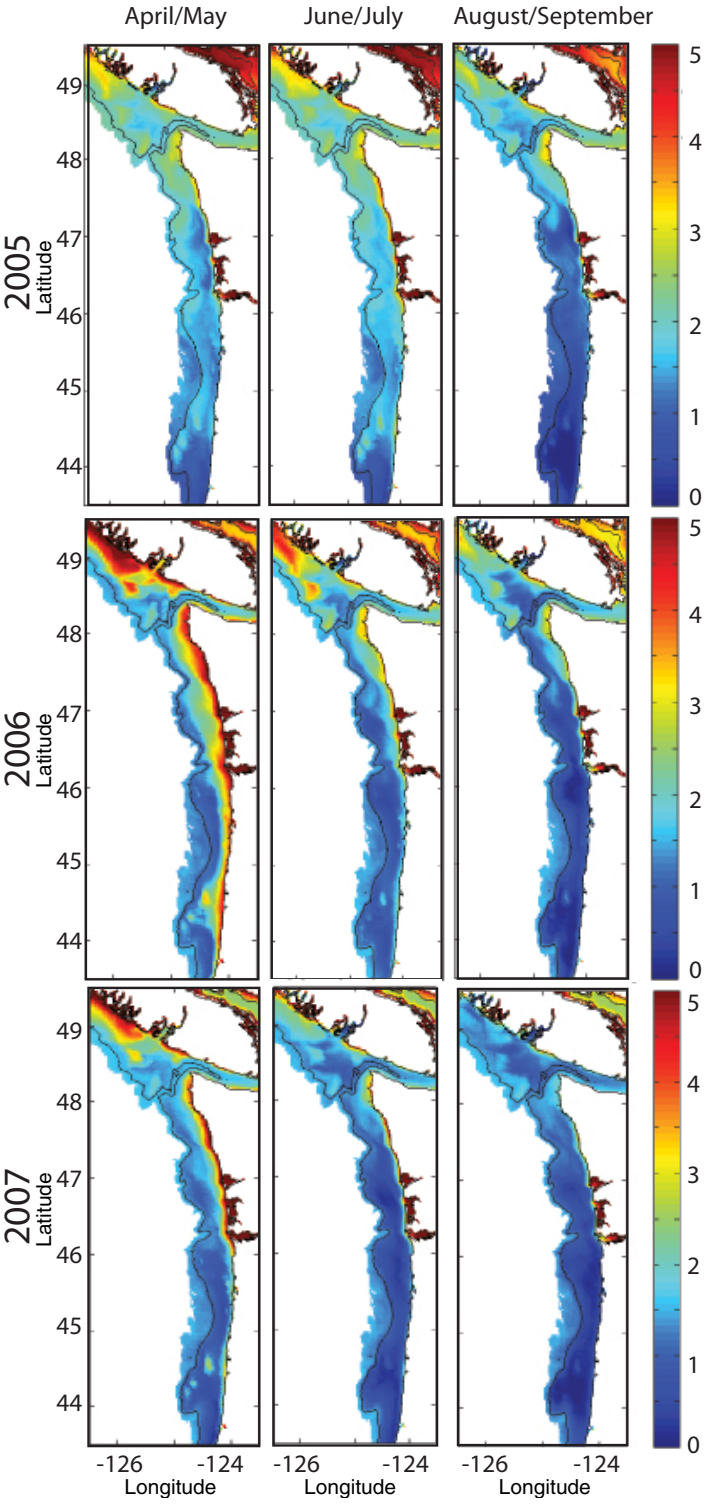

Figure 9. Time-averaged maps of bottom oxygen from the model showing the seasonal progression over the upwelling season in bottom oxygen in 2005–2007. The first column is averaged in the spring (May–April), the second column over early summer (June–July), and the last column over the late summer (August–September). Units are mL/L and the shelf break (200 m) is identified as the black contour.

the Oregon shelf, *Reimers et al.* [2012] reports sediment oxygen demand fluxes of 3.2–9.8 mmol O_2 m^{-2} d^{-1} at 80 m depth. The observations of *Hartnett and Devol* [2003] were made at a range of depths on the outer shelf and slope, as seen in Figure 11. A significant depth-dependence is observed with more sediment oxygen demand in the shallower depths. While observations of sediment oxygen demand shallower than 70 m are not available, biomass is more concentrated near the coast, which results in more large detrital particles. The larger detritus sinks faster, so it reaches the bed and respires faster. In addition, more detritus reach the bed faster, in general, in shallower water columns, as there is less area to respire in the water column. The model successfully captures the observed depth dependence (Figure 11). The shelf geometry differs between Washington and Oregon such that Washington's shelf contains a larger area of shallow (<60 m) shelf (Figure 11) [*Hickey and Banas*, 2008]. Figure 12 indicates the latitudinal trend in the shallow shelf area, mainly that the Washington shelf contains a larger area of shallow shelf than the Oregon shelf. The broader shallow shelf area on the Washington shelf likely contributes to the spatial variability of sediment oxygen demand in the model. A significant ($R^2 = 0.54$) relationship exists between the fraction of shelf area shallower than 60 m and the sediment oxygen demand (Figure 12).

3.5. Oxygen Budget for Washington Shelf

The oxygen budget for the Washington shelf region (Table 2; see Figure 1 for bounds of analysis regions) is consistent with the observation-based conclusions of *Connolly et al.* [2010], namely that respiration of organic matter locally is the dominant driver for the summer-fall oxygen decline. Each

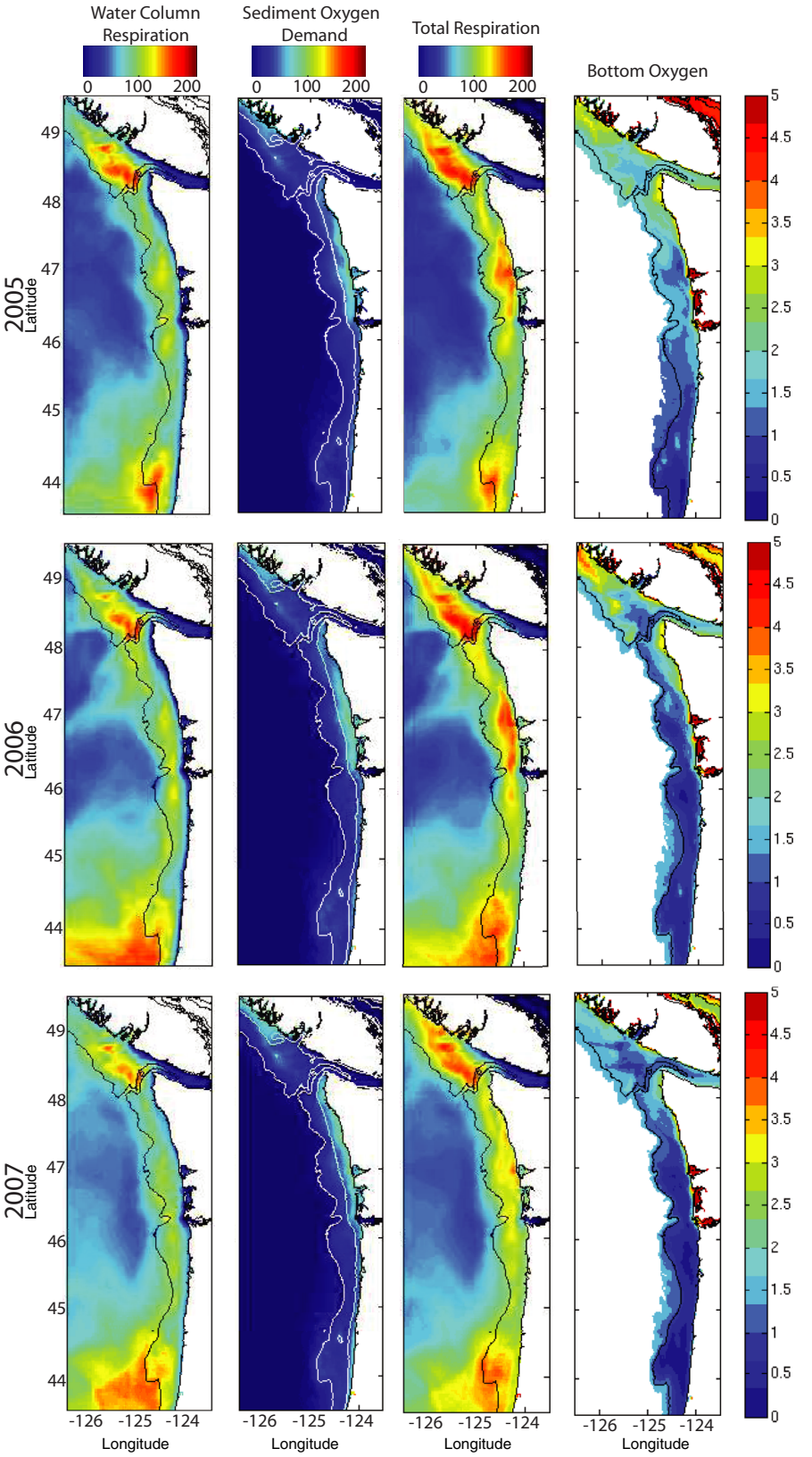

Figure 10. Time-averaged (June–September) maps of (first column) integrated water column respiration (0–200 m) (mmol O_2 m^{-2} d^{-1}), (second column) sediment oxygen demand of the sediments (mmol O_2 m^{-2} d^{-1}), total respiration (water column respiration plus sediment oxygen demand, 0–200 m) (mmol O_2 m^{-2} d^{-1}), and average bottom (0–500 m) oxygen distribution (mL/L) for (top) 2005, (middle) 2006, and (bottom) 2007. All panels include the 200 m isobaths for reference, but the sediment oxygen demand panels also include the 60 m isobath.

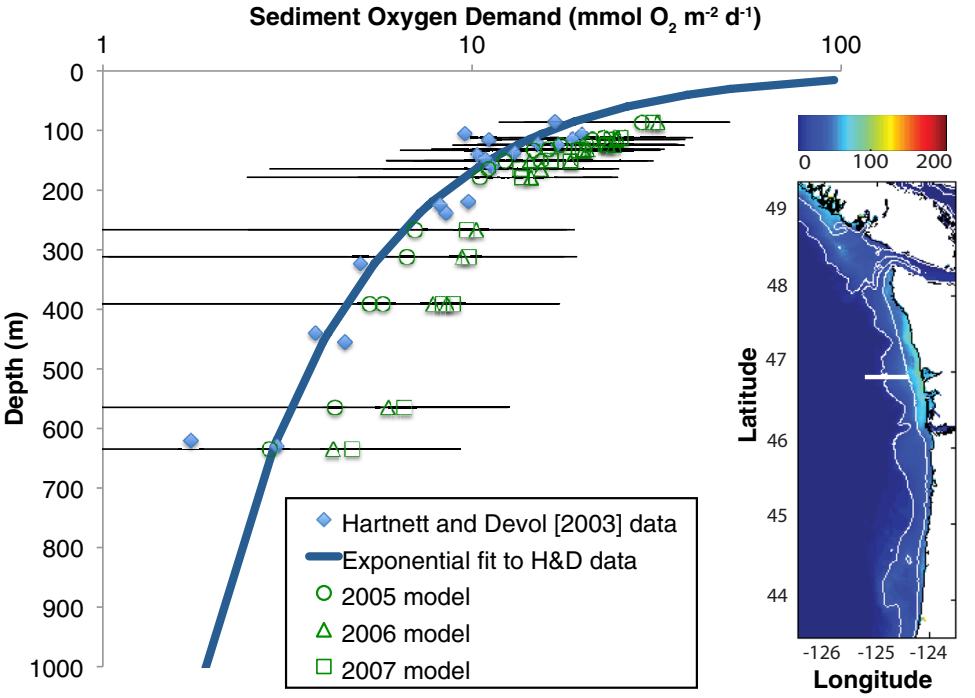

Figure 11. Sediment oxygen demand (mmol O_2 m^{-2} d^{-1}) from the model (open markers) and observations of *Hartnett and Devol* [2003] from several periods during the 1990s (filled diamonds and line) over a range of depths between 80 and 1000 m along a line depicted on the map insert. The map insert is a map of the sediment oxygen demand from the model averaged over the upwelling season in 2005. Model results are averaged over the entire upwelling season (June–September), the standard deviation of that location is plotted on each point as well.

upwelling season, 70–80% of the organic matter produced on the shelf is respired locally in the water column and in the sediments. *Connolly et al.* [2010] showed that the water column and sediments were determined to each contribute 40–60% of the oxygen consumption on the Washington shelf in 32 m of water. The model results are averaged over the whole shelf, while the results from *Connolly et al.* [2010] are for the inner shelf only. The benthic contribution to respiration declines with depth [*Hartnett and Devol*, 2003], and so the numbers presented here are somewhat smaller than reported in *Connolly et al.* [2010].

The divergence of low-oxygen water into the region varies from year to year. In 2005, the divergence term contributed more to the oxygen decline than in any of the other years, nearly equivalent to the respiration term. In 2007, the divergence term contributed the least to the oxygen decline on the shelf, contributing approximately half as much as in other years. The divergence term experiences the largest variability of all the terms in the budget.

3.6. Oxygen Budget for Oregon Shelf

The oxygen budget for the Oregon shelf region shaded in Figure 1 (Heceta Bank) illustrates the contribution of local respiration of organic matter to the seasonal oxygen decline, as on the Washington shelf, consistent with the results of *Adams et al.* [2013] (Table 2). Local respiration accounts for 87–90% of the primary production in the Oregon analysis region. The majority of the respiration occurs in the water column rather than in the sediments because the majority of the contribution to respiration comes from the small detrital pool, which respires in the upper 200 m of the water column (given the sinking velocity and respiration rate—see section 2.3), and the shelf is deep in this region. A larger percentage of the organic matter is respired locally in Oregon than in Washington likely due to the retentive nature of Heceta Bank. The primary production and respiration terms experience the most interannual variability in the oxygen budget for Oregon.

In contrast to the Washington shelf, divergence of deoxygenated water into the Oregon region is a small component of the seasonal oxygen decline. The Oregon shelf includes Heceta Bank, a previously identified semiretentive region [*Barth et al.*, 2005; *Kim and Barth*, 2011]. Retentive regions are expected to experience

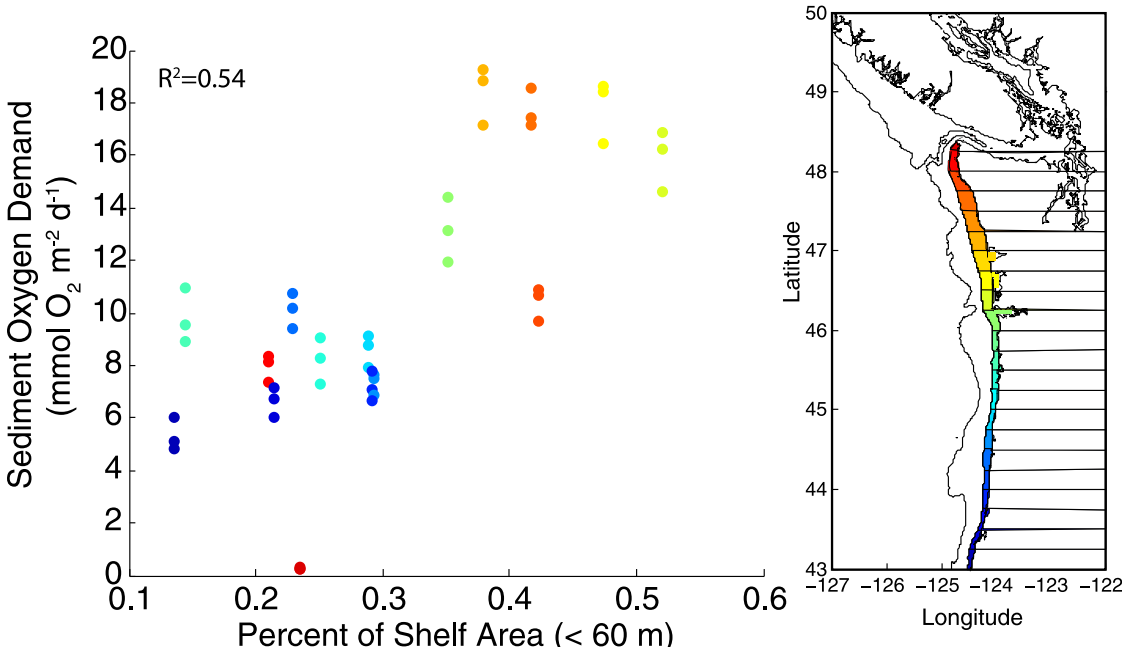

Figure 12. Sediment oxygen demand (mmol O_2 m^{-2} d^{-1}) from the model and percentage of shelf area less than 60 m deep. Model results are averaged over the entire upwelling season (June–September) and points are colored by latitude. The larger the region of shallow shelf, the more sediment oxygen demand exists in that region ($R^2 = 0.54$). A larger region of shallow shelf exists in Washington than in Oregon.

a smaller influence from the divergence term, as the circulation transit time through these regions is longer than in surrounding regions.

Another significant difference between the Washington and Oregon shelves lies in the air-sea gas exchange contribution to the oxygen budget. The model results for Oregon (0.4 mmol m^{-3} d^{-1}) on average experience 30% less degassing than the observations from 2001 of *Hales et al*. [2006] (0.64 mmol m^{-3} d^{-1} $-0.17 + 0.09$). However, if we compare only 2007 to the 2001 results, as both years experienced similar Cumulative Upwelling Index (CUI, -3.0 versus -2.8 N m^{-2} d), and average only May and August 2007 from the model to be consistent with the observations, for example, that difference is reduced to 6%. In the model, the loss of oxygen is consistently larger in Oregon than Washington. Oregon's coast experiences a larger area of cold upwelled water exposed at the sea surface than the Washington coast due to stronger winds in the region [e.g., *Giddings et al*., 2014] (Figure 6). Gas exchange is a function of the gradient between the surface oxygen concentration and the saturation concentration, which is controlled by the temperature of the water, and the wind speed. A larger region of cold water at the surface would result in a larger gradient in oxygen between the concentration in the water and the atmosphere, and consequently a larger loss.

The seasonal temporal change in oxygen in the model is similar in all 3 years reported here, consistent with observations from the Oregon shelf between 2009 and 2011 reported by *Adams et al*. [2013]. The modeled summer-fall temporal change in oxygen over the Oregon shelf of -0.3 mmol m^{-3} d^{-1}, is smaller than that reported in *Hales et al*. [2006] from 2001 (-0.61 mmol m^{-3} d^{-1} (± 0.12)) or by *Adams et al*. [2013] (-0.4 mmol m^{-3} d^{-1}). The value reported in the budget is averaged over the entire region outlined in Figure 1 and the observations from *Adams et al*. [2013], for example, were from a mooring location in 70 m of water on Heceta Bank over a different year. Despite the slight underestimate of oxygen decline, the model does exhibit significant skill in the region, as shown in Figure 5 (NOAA cruises, identified geographically in Figure 1).

3.7. Variability in Both Budgets

Time series of the terms in the oxygen budget over the upwelling season for the outlined regions on the Washington and Oregon shelves (see Figure 1) are plotted in Figure 13. The time series were integrated over the water column (0–500 m) and the shaded regions in Figure 1, and then low-pass filtered with a 30

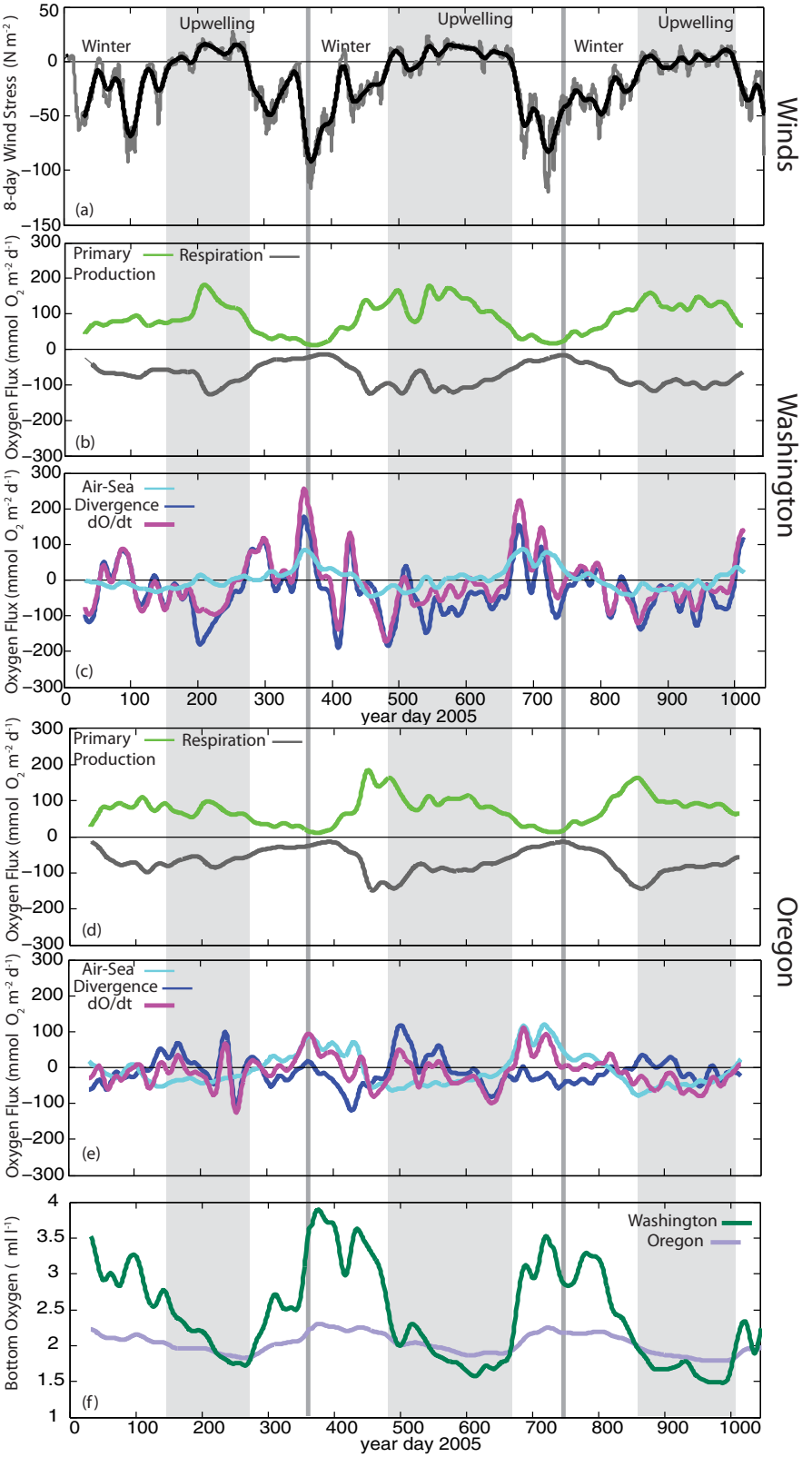

Figure 13. Time series of budget terms from the model in the boxed regions from Table 2 for (top) Washington and (bottom) Oregon from 2005–2007. Time series were vertically integrated over the top 500 m of water and then filtered with a Hanning filter using a 30 day window. Upwelling seasons, as determined by the 8 day upwelling index for the Washington shelf [*Austin and Barth*, 2002] plotted as a black line, are shaded as gray. Both Oregon and Washington experience the same transitions, despite the difference in the magnitude of the wind stress. Oregon experiences stronger winds.

day Hanning window to focus on the seasonal variability. The seasonality of the respiration and production terms of the oxygen budget on both shelves is clearly evident with maxima in production and respiration occurring during the upwelling season in all 3 years. The time series also confirm the results from Table 2 for the budget. For example, that primary production and respiration are the biggest terms on average in the budget.

The variability of the other terms in the budget throughout the year differs for each term. The divergence term exhibits the most variability throughout the record. The divergence term varies seasonally, as well as spatially (Figure 13). In Washington, the maximum occurs in winter, and the divergence term is mostly a loss of oxygen over the upwelling season. In Oregon, the contribution of the divergence term varies from year to year with no clear trend seasonally. The dO/dt term follows divergence closely, and divergence appears to vary independent of production and respiration (Figure 13). In Washington, one of biggest contributions to variability in the oxygen budget comes from the divergence term; however, in both regions, divergence has the biggest standard deviation over the upwelling season (Table 2).

4. Discussion

Observations and model results show that oxygen is drawn down in the study region over the upwelling season. The modeled budgets for all 3 years indicate that local respiration and divergence, or circulation, contribute similar (60 versus 40%) amounts to integrated oxygen budget on the Washington coast while respiration dominates the Oregon coast in the Heceta Bank region. In addition to the direct effect of circulation in the oxygen budget, the circulation influences the oxygen budget through mechanisms of recirculation on the shelf which cause regional hot spots of respiration, as we discuss below. Most of the mechanisms of recirculation and retention have been previously identified in the literature [*Tully*, 1941; *Denman and Freeland*, 1985; *Hickey and Banas*, 2003, 2008; *Foreman et al*., 2008; *Marchetti et al*., 2004; *MacFadyen et al*., 2005, 2008; *Venegas et al*., 2008; *Trainer et al*., 2009; *Kim and Barth*, 2011], but their role in the development of regional hot spots for hypoxia and its interannual variability have not been previously addressed. In the discussion that follows, the details of the oxygen budget and the influence of recirculation in the region on regional patterns of hypoxia are discussed in further detail.

4.1. Spatial Patterns of Respiration, Low Oxygen, and Retention

Patterns of respiration vary spatially along the coasts of Washington, Oregon, and British Columbia (Figure 10). Regions with the highest respiration coincide with locations of persistent hypoxia across all 3 years of simulations. As previously discussed, the three regions of intense respiration include Heceta Bank, the Washington shelf region offshore of Grays Harbor (46°N–47°N), and the region beneath the Juan de Fuca Eddy (Figure 10). Each of these regions is a "hot spot" of organic matter respiration for a different reason. Heceta Bank and the Juan de Fuca Eddy are well-known semiretentive regions [*Tully*, 1941; *Denman and Freeland*, 1985; *Hickey and Banas*, 2003, 2008; *Foreman et al*., 2008; *Marchetti et al*., 2004; *MacFadyen et al*., 2008; *Trainer et al*., 2009; *Venegas et al*., 2008; *MacFadyen and Hickey*, 2010; *Kim and Barth*, 2011]. In both regions, longer residence times than typical of open coast shelf regions have been observed due to local recirculation patterns. In the Juan de Fuca eddy region, retention has been observed up to 32 days [*Hickey and Banas*, 2008; *MacFadyen and Hickey*, 2010; *Giddings et al*., 2014]. Both the Juan de Fuca eddy region and Heceta Bank coincide with regions of high vertically integrated water column respiration (Figure 10, first column), which is consistent with longer residence times in these regions. The Washington open shelf appears as a third region of high vertically integrated total respiration (Figure 10, third column), when the water column respiration (Figure 10, first column) is added to the sediment oxygen demand, i.e., respiration at the sediment-water interface (Figure 10, second column). The oxygen budget results confirm that the contribution of sediment oxygen demand to the seasonal decline of oxygen is larger on the Washington shelf than it is on the Oregon shelf, where water column respiration is more important (Table 2).

Our results suggest that the width of shallow shelf is the key metric controlling sediment oxygen demand. We hypothesize that the proximity of the bottom to the surface on shallow shelves allows a large percentage of organic matter to reach the seafloor. Because of the model formulation, sediment oxygen demand is directly proportional to the sinking flux of detritus that reaches the bottom. Once near the bottom,

nutrients remain on the shelf until they are physically flushed from the region. Thus, the relatively large area of shallow shelf off the central and southern WA coast could explain this area's susceptibility to hypoxia. "Retention" in this case occurs due to weak cross-shelf export over a relatively wider shelf, even if the region does not show clear local recirculation patterns like the Juan de Fuca Eddy or Heceta Bank. Given that detrital concentrations are high in the region off Grays Harbor and sediment oxygen demand is also high, it is likely that both cross-shelf export and shallow shelf area mechanisms are important.

4.1.1. What is the Role of the Columbia River?

The Washington shelf is occupied by the Columbia River plume 50% or more of the summer, despite the plume's reduced influence and typical position extending offshore and southward during the summer upwelling months [*Hickey et al*., 2005]. The Columbia River plume has been observed under different conditions to both increase export of organic material at the surface [*Banas et al*., 2009b], as well as, increase retention near the river mouth [*Kudela et al*., 2010] and on the inner shelf [*Banas et al*., 2009b; *Hickey and Banas*, 2003]. In the same model years described here, the Columbia River discharge was set to zero and compared to the complete system to determine the effect of the plume (see *Giddings et al*. [2014] for further discussion). Overall, the runs without the Columbia River were slightly (∼2%) higher in oxygen on the Washington shelf. This difference was most pronounced during late winter upwelling events. Over the summer upwelling season, oxygen on the inner shelf was 5–20% higher on average at EH4 in the case without the Columbia River. In 2006, the year with the largest discharge of the three, the biggest difference resulted. Although, the Columbia River plume presence may play an additional role in determining the oxygen levels on the Washington shelf, it does not contribute to the spatial pattern of high respiration offshore of Grays Harbor.

4.1.2. What About Regions That Rarely Experience Hypoxia?

Some regions *rarely* experience hypoxia despite having high productivity; e.g., the region north of Grays Harbor, but south of the Strait of Juan de Fuca (between 47°N and 48°N). In an experiment where the Strait of Juan de Fuca was closed, eliminating exchange with Puget Sound, the normoxic zone expanded in the region (see *Davis et al.* [2014], for further discussion). This suggests that some aspect of the exchange with the estuary is correlated with the magnitude and extent of the normoxic zone on the Washington coast. One possibility is that shutting off the outflow from the Strait of Juan de Fuca, which is an important nutrient source for the Washington shelf [*Davis et al*., 2014], decreases organic matter production, which reduces local respiration processes as well. Consequently, oxygen is higher on the Washington shelf when the exchange with the estuary is shut down.

4.2. When is Circulation More Important Than Respiration to Oxygen Dynamics on the Shelf?

The divergence, or circulation term encompasses all vertical and horizontal advection processes including the poleward undercurrent, eddies, and wind-driven circulation. The terms in the budget in Figure 13 and in Table 2 are integrated in time as well as vertically integrated over the whole shelf and upper slope down to 500 m. As a result, the local dynamics as well as large-scale processes are integrated into this term. It is beyond the scope of this paper to separate each of these processes individually, but will be the focus of future research. However, some conclusions about dominant processes can be drawn from Figure 13 as well as Figure 14. First, the variability on the order of tens of days in the circulation explains a lot of the variability in the dO/dt term. This variability could be driven by any of the processes described above that influence the local circulation. Because the variability in the divergence term over the entire shelf region is correlated to the variability at an inner shelf location (mooring at EH4, Figure 14), the process governing this variability is most likely three-dimensional wind-driven circulation. The corresponding wind stress varies with the divergence, which is consistent with this idea (Figure 14).

5. Summary and Conclusions

Here we have presented results from a regional model with extensive validation of physical, chemical and biological constituents to separate the physical and biological variability contributing to bottom hypoxia in the region over a 3 year period. A large regional data set (thousands of CTDs with nutrients, tens of moored arrays) has been used to constrain the model with sufficient skill to capture spatial and temporal patterns of dissolved oxygen in the North American Pacific Northwest coastal ocean. The model was added to an existing circulation and ecosystem model framework that includes the Salish Sea [*Giddings et al*., 2014; *Davis*

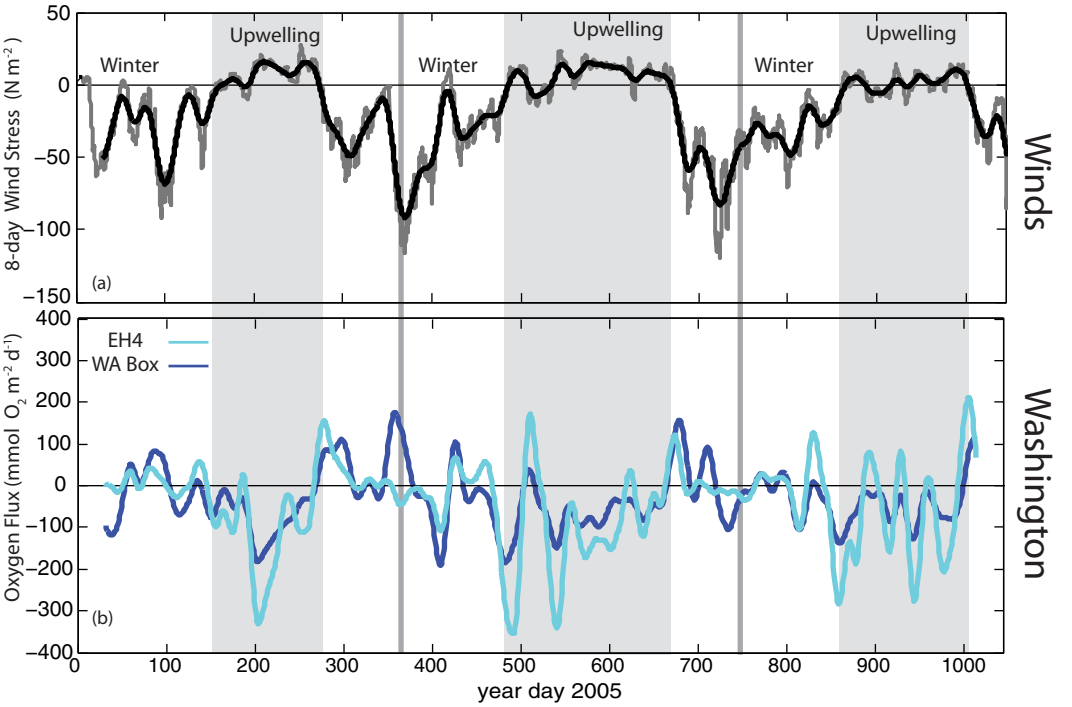

Figure 14. Time series of divergence term from the model oxygen budget for the Washington coast boxed regions and for the mooring location at EH4 (32 m) from 2005 to 2007. Time series were vertically integrated over the top 500 m of water or water column depth and then filtered with a Hanning filter using a 30 day window. Upwelling seasons, as determined by the 8 day upwelling index [*Austin and Barth*, 2002] plotted as a black line, are shaded as grey.

et al., [2014]. New model elements were added here to develop the oxygen model including a second detrital class and improved detrital dynamics with the elimination of burial, both constrained by local observations.

Overall, the model results show that:

1. Respiration and divergence contribute similar (60 versus 40%) amounts to integrated oxygen budget on the Washington coast while respiration dominates the Oregon coast.
2. Spatial variability of hypoxia is determined by the spatial variability of respiration on the shelf, which is influenced by local recirculation processes.
3. Water column respiration is more important in recirculation regions like the Juan de Fuca Eddy and Heceta Bank, while sediment oxygen demand is more important in areas such as the Washington coast with a greater extent of shallow (<60 m) shelf.
4. Divergence of oxygen dominates the variability in the rate of oxygen decline over a season.

After the onset of seasonal upwelling, respiration of organic matter produced locally on the shelf controls the seasonal decline of oxygen. This seasonal decline, as well as spatial variability in oxygen, is well represented by the model. Retentive physical features like the Juan de Fuca eddy and Heceta Bank emerge from the spatial maps of respiration, and persistently develop hypoxia. The hypoxic region on Washington's shelf develops as a result of the large shallow shelf area.

Modeled oxygen consistently predicted fluctuations on both seasonal and event time scales. The reasonable results explicitly confirm several assumptions, for example, the need for more than one detrital pool, the importance of settling velocities, as well as the underlying biological interactions such as the production and maintenance of a large standing stock of biomass on the shelf. Future work should focus on interannual variability in source water chemistry, constraining spatial variability in respiration and identifying processes responsible for the spatial variability in retention. Understanding those processes is crucial to our ability to predict future trends in hypoxia in this region.

Appendix A

More information about the ecosystem model can be found in *Banas et al*. [2009b] and *Davis et al*. [2014].

Ecosystem model equations:

$$\frac{\partial P}{\partial t} = \mu_i(E,N)P - I(P)Z - mP + advection + diffusion \tag{A1a}$$

$$\frac{\partial Z}{\partial t} = \varepsilon I(P)Z - \xi Z^2 + advection + diffusion \tag{A1b}$$

$$\frac{\partial SD}{\partial t} = (1-\varepsilon) f_{egest} I(P)Z + mP + \xi Z^2 - rSD - \tau(SD)^2 - w_{SD}\frac{\partial SD}{\partial z} + advection + diffusion \tag{A1c}$$

$$\frac{\partial LD}{\partial t} = \tau(SD)^2 - rLD - w_{LD}\frac{\partial LD}{\partial z} + advection + diffusion \tag{A1d}$$

$$\frac{\partial N}{\partial t} = -\mu_i(E,N)P + (1-\varepsilon)(1-f_{egest})I(P)Z + rSD + rLD - F^{benthic}_{denitr} - F^{wc}_{denitr} + advection + diffusion \tag{A1e}$$

Model parameter definitions and units are given in Table 1. Phytoplankton growth rate (μ_i) is limited by light availability and the uptake of nutrients (equation (A2)). We calculate the nutrient uptake rate with a formulation that allows for differentiation of the half saturation for nutrient uptake (k_s) between the high-nutrient shelf conditions and low-nutrient open ocean conditions [*Smith et al*., 2009]:

$$\mu_i(E,N) = \mu_0 \frac{N}{k_{s,app} + N} \frac{\alpha E}{\sqrt{\mu_0^2 + \alpha^2 E^2}} \tag{A2}$$

where

$$k_{s,app} = k_s + 2\sqrt{k_s N}$$

Photosynthetically available radiation (PAR or E in equation (A3)) at depth z is a function of light attenuation due to the optical properties of seawater and self-shading by phytoplankton. Light attenuation parameters (att_{sw} and att_P) are derived from PAR, chlorophyll *a*, and salinity measurements from 43 CTD casts taken between 45.5°N and 47.5°N during the 2004–2005 RISE cruises. A salinity dependence in the formulation for att_{sw} (see Table 1) is used to express the varying optical properties of different water types within our domain (river plume, estuarine, open ocean) as described by the CTD PAR measurements.

$$E(z) = E_{surface} \exp\left(att_{sw}(S)z + att_P \int_z^{surface} P(z')dz' \right) \tag{A3}$$

After *Banas et al*. [2009a], the functional form for zooplankton ingestion $I(P)$ (in equation (A1b)) includes a quadratic prey saturation response (equation (A4)), where K_s is a half saturation coefficient and total zooplankton ingestion is divided into zooplankton net growth, excretion, and egestion using two parameters, e and f_{egest} (Figure 2).

$$I(P) = I_0 \frac{P^2}{K_s^2 + P^2} \tag{A4}$$

The benthic denitrification flux, applied to the deepest grid layer only, is

$$F^{benthic}_{denitr}|_{z=-H} = min\left(\frac{\chi}{\Delta z}, w_{SD}\frac{\partial SD}{\partial z}|_{z=-H} + w_{LD}\frac{\partial LD}{\partial z}|_{z=-H} \right) \tag{A5}$$

where χ is 1.2 mmol N m^{-2} d^{-1} [*Hartnett and Devol*, 2003] and Δz the grid layer depth. This formulation limits its benthic denitrification to be no greater than the current flux of organic matter to the benthos, a threshold which is typically reached around the 1000 m isobath in our model. Water-column denitrification is formulated so that when dissolved oxygen concentration [O_2] is too low to support the bacterial respiration required for the respiration flux specified in equations (A1c) and (A1d), the N pool is drawn down instead:

Acknowledgments
Special thanks to N. Kachel (CTD data) from the ECOHAB-PNW and RISE projects, E. Dever (multiyear moored sensors from the RISE project), R. Thomson (moored arrays and CTD data, Fisheries and Oceans Canada Institute of Ocean Sciences, IOS), B. Peterson (multiyear OR CTD data), the National Oceanic and Atmospheric Administration (NOAA, CTD data and tide gauges), the Olympic Coast National Marine Sanctuary (OCNMS, multiyear WA moored sensors), the Puget Sound Regional Synthesis Model (PRISM, Puget Sound CTD data), Washington State Department of Ecology (DOE, Puget Sound CTD data), King County Puget Sound Marine Monitoring (Puget Sound CTD data), and the Hood Canal citizen monitoring project (Hood Canal CTD data) and Richard Feely and Simone Alin (NOAA-PMEL, bottle data) for use of their data. Thanks to other members of the PNWTOX and UWCMG groups for useful discussions including M. Foreman, R. Thomson, I. Fine, E. Lessard, S. Lubetkin, R. McCabe, D. Sutherland, and K. Thyng. In addition, conversations with Al Devol and Burke Hales were helpful in shaping this work. Finally, we want to thank Debby Ianson and an anonymous second reviewer for their valued comments. D. Darr provided computer cluster administration and support, and computations were done on the University of Washington Hyak supercomputer system, supported in part by the University of Washington eScience Institute. This work was supported by a postdoctoral fellowship to Samantha Siedlecki from JISAO and the Program on Climate Change at the University of Washington, and grants from the Coastal Ocean Program of the National Oceanic and Atmospheric Administration (NOAA) (NA09NOS4780180) and the National Science Foundation (NSF) (OCE0942675) as part of the Pacific Northwest Toxins (PNWTOX) project. This is ECOHAB and PNWTOX contributions #812 and #14. The statements, findings, conclusions, and recommendations are those of the participants/authors and do not reflect the views of NSF, NOAA, or the Department of Commerce. Observational data from the RISE and ECOHAB PNW programs used for model validation are available through the BCO-DMO repository (http://www.bco-dmo.org/project/2094, http://www.bco-dmo.org/project/2095). NOAA data are available from CDIAC (http://cdiac.ornl.gov). Other observational data can be requested from the aforementioned sources and references cited within the manuscript.

$$F^{wc}_{denitr} = \frac{1}{c_{O:N}} max\left(c_{O:N} r(SD+LD) - \frac{O}{\Delta t}, 0\right) \quad \text{(A6)}$$

where Δt is the model time step and $c_{O:N} = 108/16$ mol:mol.

References

Adams, K. A., J. A. Barth, and F. Chan (2013), Temporal variability of near-bottom dissolved oxygen during upwelling off central Oregon, *J. Geophys. Res. Oceans*, *118*, 4839–4854, doi:10.1002/jgrc.20361.

Alford, M. H., and P. MacCready (2014), Flow and mixing in Juan de Fuca Canyon, Washington, *Geophys. Res. Lett.*, *41*, 1608–1615, doi:10.1002/2013GL058967.

Allen, S. E., and X. D. de Madron (2009), A review of the role of submarine canyons in deep-ocean exchange with the shelf, *Ocean Sci.*, *5*, 607–620, doi:10.5194/os-5-607-2009.

Allen, S. E., C. Vindeirinho, R. E. Thomson, M. G. G. Foreman, and D. L. Mackas (2001), Physical and biological processes over a submarine canyon during an upwelling event, *Can. J. Fish. Aquat. Sci.*, *58*, 671–684, doi:10.1139/f01-008.

Archer, D. E., and A. H. Devol (1992), Benthic oxygen fluxes on the Washington shelf and slope: A comparison of in situ microelectrode and chamber flux measurements, *Limnol. Oceanogr.*, *37*(3), 614–629, doi:10.4319/lo.1992.37.3.0614.

Austin, J. A., and J. A. Barth (2002), Variation in the position of the upwelling front on the Oregon shelf, *J. Geophys. Res.*, *107*(C11), 3180, doi:10.1029/2001JC000858.

Banas, N. S., E. Lessard, R. Kudela, P. MacCready, T. Peterson, B. M. Hickey and E. Frame (2009a), Planktonic growth and grazing in the Columbia River plume region: A biophysical model study, *J. Geophys. Res.*, *114*, C00B06, doi:10.1029/2008JC004993.

Banas, N. S., P. MacCready, and B. M. Hickey (2009b), The Columbia River plume as cross-shelf exporter and along-coast barrier, *Cont. Shelf Res.*, *29*, 292–301, doi:10.1016/j.csr.2008.03.011.

Barron, C. N., A. B. Kara, P. J. Martin, R. C. Rhodes, and L. F. Smedstad (2006), Formulation, implementation and examination of vertical coordinate choices in the Global Navy Coastal Ocean Model (NCOM), *Ocean Modell.*, *11*, 347–375.

Barth, J. A., S. D. Pierce, and R. M. Castelao (2005), Time-dependent, wind-driven flow over a shallow midshelf submarine bank, *J. Geophys. Res.*, *110*, C10S05, doi:10.1029/2004JC002761.

Bianucci, L., K. L. Denman, and D. Ianson (2011), Low oxygen and high inorganic carbon on the Vancouver Island Shelf, *J. Geophys. Res.*, *116*, C07011, doi:10.1029/2010JC006720.

Brewer, P. G., A. F. Hofmann, E. T. Peltzer, and W. Ussler III (2014), Evaluating microbial chemical choices: The ocean chemistry basis for the competition between use of O_2 or NO_3^- as an electron acceptor, *Deep Sea Res., Part I*, *87*, 35–42, doi:10.1016/j.dsr.2014.02.002.

Calbet, A., and M. R. Landry (2004), Phytoplankton growth, microzooplankton grazing, and carbon cycling in marine systems, Limnol. *Oceanogr. Methods*, *49*, 51–57.

Chan, F., J. A. Barth, J. Lubchenco, A. Kirincich, H. Weeks, W. T. Peterson, and B. A. Menge (2008), Emergence of anoxia in the California current large marine ecosystem, *Science*, *319*(5865), 920, doi:10.1126/science.1149016.

Christensen, J. P., J. W. Murray, A. H. Devol, and L. A. Codispoti (1987), Denitrification in continental shelf sediments has major impact on the oceanic nitrogen budget, *Global Biogeochem. Cycles*, *1*, 97–116.

Codispoti, L. A., T. Yoshinari, and A. H. Devol (2005), Suboxic respiration in the oceanic water column, in *Respiration in Aquatic Ecosystems*, edited by P. A. del Giorgio and P. J. le B. Williams, pp. 225–247, Oxford Univ. Press, Oxford, U. K.

Connolly, T. P., and B. M. Hickey (2014), Regional impact of submarine canyons during seasonal upwelling, *J. Geophys. Res. Oceans*, *119*, 953–975, doi:10.1002/2013JC009452.

Connolly, T. P., B. M. Hickey, S. L. Geier and W. P. Cochlan (2010), Processes influencing seasonal hypoxia in the northern California Current System, *J. Geophys. Res.*, *115*, C03021, doi:10.1029/2009JC005283.

Crawford, W. R., and A. Peña (2013), Declining oxygen on the British Columbia continental shelf, *Atmos. Ocean*, *51*(1), 88–103.

Davis, K. A., N. S. Banas, S. N. Giddings, S. A. Siedlecki, P. MacCready, E. J. Lessard, R. M. Kudela, and B. M. Hickey (2014), Estuary-enhanced upwelling of marine nutrients fuels coastal productivity in the U.S. Pacific Northwest, *J. Geophys. Res. Oceans*, *119*, doi:10.1002/2014JC010248.

Denman, K. L., and H. J. Freeland (1985), Correlation scales, objective mapping and a statistical test of geostrophy over the continental shelf, *J. Mar. Res.*, *43*(3), 517–539, doi:10.1357/002224085788440402.

Devol, A. (1991), Direct measurements of nitrogen gas fluxes from continental shelf sediments, *Nature*, *349*, 319–321.

Devol, A. H., and J. P. Christensen (1993), Benthic fluxes and nitrogen cycling in sediments of the continental margin of the eastern North Pacific, *J. Mar. Res.*, *51*, 345–372.

DeVries, T., C. Deutsch, P. A. Rafter, and F. Primeau (2012), Marine denitrification rates determined from a global 3-dimensional inverse model, *Biogeosci. Discuss.*, *9*, 14,013–14,052, doi:10.5194/bgd-9-14013-2012.

Dunne, J. P., J. W. Murray, J. Young, L. Balistrieri, and J. K. B. Bishop (1997), ^{234}Th and particle cycling in the central equatorial Pacific, *Deep Sea Res., Part II*, *44*, 2049–2083.

Emery, W. J., and R. E. Thomson (2004), *Data Analysis Methods in Physical Oceanography*, 2nd ed., Elsevier, Amsterdam.

Fennel, K., J. Wilikin, J. Levin, J. Moisan, J. O'Reily, and D. Haidvogel (2006), Nitrogen cycling in the Middle Atlantic Bight: Results from a three-dimensional model and implications for the North Atlantic nitrogen budget, *Global Biogeochem. Cycles*, *20*, GB3007, doi:10.1029/2005GB002456.

Foreman, M. G. G., W. Callendar, A. MacFadyen, B. M. Hickey, R. E. Thimson and E. D. Lorenzo (2008), Modeling the generation of the Juan de Fuca Eddy, *J. Geophys. Res.*, *113*, C03006, doi:10.1029/2006JC004082.

Garcia, H. E., and L. I. Gordon (1992), Oxygen solubility in seawater: Better fitting equations, *Limnol. Oceanogr.*, *37*(6),1307–1312.

Giddings, S., P. MacCready, B. Hickey, N. Banas, K. Davis, S. Siedlecki, V. Trainer, R. Kudela, N. Pelland, and T. Connolly (2014), Hindcasts of harmful algal bloom transport on the Pacific Northwest coast, *J. Geophys. Res. Oceans*, *119*, 2439–2461, doi:10.1002/2013JC009622.

Grantham, B. A., F. Chan, K. J. Nielsen, D. S. Fox, J. A. Barth, A. Huyer, J. Lubchenco and B. A. Menge (2004), Upwelling-driven nearshore hypoxia signals ecosystem and oceanographic changes in the northeast Pacific, *Nature*, *429*, 749–754, doi:10.1038/nature02605.

Groussart, H., and H. Ploug (2001), Microbial degradation of organic carbon and nitrogen on diatom aggregates, *Limnol. Oceanogr.*, *46*(2), 267–277.

Mooring data are available from http://coast.ocean.washington.edu. Model run setup files and output used in this manuscript are available upon request from Parker MacCready (parker@ocean.washington.edu). The statements, findings, conclusions, and recommendations are those of the participants/authors and do not reflect the views of NSF, NOAA, or the Department of Commerce.

Hales, B., L. Karp-Boss, A. Perlin, and P. Wheeler (2006), Oxygen production and carbon sequestration in an upwelling coastal margin, Global Biogeochem. *Cycles*, *20*, GB3001, doi:10.1029/2005GB002517.

Hansen, P. J., P. K. Bjornsen, and B. W. Hansen (1997), Zooplankton grazing and growth: Scaling within the 2–2000 um body size range, *Limnol. Oceanogr.*, *42*(4), 687–704.

Hartnett, H. E., and A. H. Devol (2003), Role of a strong oxygen-deficient zone in the preservation and degradation of organic matter: A carbon budget for the continental margins of northwest Mexico and Washington State, *Geochim. Cosmochim. Acta*, *67*(2), 247–264.

Healey, K., A. H. Monahan, and D. Ianson (2009), Perturbation dynamics of a planktonic ecosystem, *J. Mar. Res.*, *67*, 637–666.

Hedges, J. I., and R. G. Keil (1995), Sedimentary organic matter preservation: An assessment and speculative synthesis, *Mar. Chem.*, *49*, 81–115.

Hickey, B. M. (1979), The California Current System—Hypotheses and facts, *Prog. Oceanogr.*, *8*(4), 191–279, doi:10.1016/0079-6611(79)90002-8.

Hickey, B. M. (1984), The fluctuating alongshore pressure gradient on the Pacific Northwest shelf: A dynamical analysis. *J. Phys. Oceanogr.*, 14, 276–293.

Hickey, B. M. (1989), Patterns and processes of shelf and slope circulation, in *Coastal Oceanography of Washington and Oregon*, edited by M. R. Landry and B. M. Hickey, pp. 41–115, Elsevier Sci., Amsterdam.

Hickey, B. M. (1998), Coastal oceanography of western North America from the tip of Baja California to Vancouver Island: Coastal segment, in *The Sea*, vol. 11, edited by A. R. Robinson and K. H. Brink, pp. 345–391, John Wiley, Amsterdam, Netherlands.

Hickey, B. M. and N. S. Banas (2003), Oceanography of the US Pacific Northwest Coastal Ocean and estuaries with application to coastal ecology, *Estuaries*, *26*, 1010–1031.

Hickey, B., S. Geier, N. Kachel, and A. MacFadyen (2005), A bi-directional river plume: The Columbia in summer, *Cont. Shelf Res.*, *25*, 1631–1656.

Hickey, B. M. and N. S. Banas (2008), Why is the northern end of the California Current System so productive?, *Oceanography*, *21*(4), 90–107.

Hickey, B. M., et al. (2010), River influences on shelf ecosystems: Introduction and synthesis, *J. Geophys. Res.*, *115*, C00B17, doi:10.1029/2009JC005452.

Hill, A. E., B. M. Hickey, F. A. Shillington, P. T. Strub, K. H. Brink, E. D. Barton, and A. C. Thomas (1998), Eastern ocean boundaries, in *The Sea*, vol. 11, edited by A. R. Robinson and K. H. Brink, pp. 29–67, John Wiley, Amsterdam, Netherlands.

Huyer, A. (1983), Coastal upwelling in the California Current System, *Prog. Oceanogr.*, *12*(3), 259–284, doi:10.1016/0079-6611(83)90010-1.

Huyer, A., E. J. C. Sobey, and R. L. Smith (1979), The spring transition in currents over the Oregon Continental Shelf, *J. Geophys. Res.*, *84*, 6995–7011, doi:10.1029/JC084iC11p06995.

Ianson, D., and S. E. Allen (2002), A two-dimensional nitrogen and carbon flux model in a coastal upwelling region, *Global Biogeochem. Cycles*, *16*(1), 1011, doi:10.1029/2001GB001451.

Ianson, D., S. E. Allen, S. L. Harris, K. J. Orians, D. E. Varela, and C. S. Wong (2003), The inorganic carbon system in the coastal upwelling region west of Vancouver Island, Canada, *Deep Sea Res., Part I*, *50*(8), 1023–1042.

Ianson, D., C. Völker, K. L. Denman, E. Kunze, and N. Steiner (2012), The effect of vertical and horizontal dilution on fertilized patch experiments, *Global Biogeochem. Cycles*, *26*, GB3002, doi:10.1029/2010GB004008.

Iversen, M. H., and H. Ploug (2010), Ballast minerals and the sinking carbon flux in the ocean: Carbon-specific respiration rates and sinking velocity of marine snow aggregates, *Biogeosciences*, *7*, 2613–2624, doi:10.5194/bg-7-2613-2010.

Iverson, M. H., and H. Ploug (2013), Temperature effects on carbon-specific respiration rate and sinking velocity of diatom aggregates—Potential implications for deep ocean export processes, *Biogeosciences*, *10*, 4073–4085, doi:10.5194/bg-10-4073-2013.

Jackson, G. A., A. M. White, and P. W. Boyd (2005), Role of algal aggregation in vertical carbon export during SOIREE and in other low biomass environments, *Geophys. Res. Lett.*, *32*, L13607, doi:10.1029/2005GL023180.

Jolliff, J. K., J. C. Kindle, I. Shulman, B. Penta, M. A. M. Friedrichs, and R. A. Arnone (2009), Summary diagrams for coupled hydrodynamic-ecosystem model skill assessment, *J. Mar. Syst.*, *76*, 64–82, doi:10.1016/j.jmarsys.2008.05.014.

Kim, S., and J. A. Barth (2011), Connectivity and larval dispersal along the Oregon coast estimated by numerical simulations, *J. Geophys. Res.*, *116*, C06002, doi:10.1029/2010JC006741.

Kosro, P. M., W. T. Peterson, B. M. Hickey, R. K. Shearman and S. D. Pierce (2006), Physical versus biological spring transition: 2005, *Geophys. Res. Lett.*, *33*, L22S03, doi:10.1029/2006GL027072.

Kudela, R. M., S. Seeyave, and W. P. Cochlan (2010), The role of nutrients in regulation and promotion of harmful algal blooms in upwelling systems, *Prog. Oceanogr.*, *85*(1–2), 122–135, doi:10.1016/j.pocean.2010.02.008.

Landry, M. R., J. R. Postel, W. K. Peterson, and J. Newman (1989), Broad-scale patterns in the distribution of hydrographic variables, in *Coastal Oceanography of Washington and Oregon*, edited by M. R. Landry and B. M. Hickey, pp. 1–40, Elsevier Sci., Amsterdam.

Levin, L. A., W. Ekau, A. J. Gooday, F. Jorissen, J. J. Middelburg, W. Naqvi, C. Neira, N. N. Rabalais, and J. Zhang (2009), Effects of natural and human-induced hypoxia on coastal benthos, *Biogeosciences*, *6*(2), 2063–2098, doi:10.5194/bg-6-2063-2009.

Lima, I. D., and S. C. Doney (2004), A three-dimensional, multinutrient, and size-structured ecosystem model for the North Atlantic, *Global Biogeochem. Cycles*, *18*, GB3019, doi:10.1029/2003GB002146.

Lynn, R. L., and J. J. Simpson (1987), The California Current System: The seasonal variability of its physical characteristics, *J. Geophys. Res.*, *92*, 12,947–12,966, doi:10.1029/JC092iC12p12947.

Macdonald, R. W., and T. F. Pedersen (1991), Geochemistry of sediments of the western Canadian continental shelf, *Cont. Shelf Res.*, *11*, 717–735.

MacFadyen, A., and B. M. Hickey (2010), Generation and evolution of a topographically linked, mesoscale eddy under steady and variable wind-forcing, *Cont. Shelf Res.*, *30*(13), 1387–1402.

MacFadyen, A., B. M. Hickey and M. G. G. Foreman (2005), Transport of surface waters from the Juan de Fuca eddy region to the Washington coast, *Cont. Shelf Res.*, *25*(16), 2008–2021.

MacFadyen, A., B. M. Hickey and W. P. Cochlan (2008), Influences of the Juan de Fuca Eddy on circulation, nutrients, and phytoplankton production in the northern California Current System, *J. Geophys. Res.*, *113*, C08008, doi:10.1029/2007JC004412.

Marchetti, A., V. L. Trainer, and P. J. Harrison (2004), Environmental conditions and phytoplankton dynamics associated with Pseudo-nitzschia abundance and domoic acid in the Juan de Fuca eddy, *Mar. Ecol. Prog. Ser.*, *281*, 1–12, doi:10.3354/meps281001.

Mass, C. F., et al. (2003), Regional environmental prediction over the Pacific Northwest, *Bull. Am. Meteorol. Soc.*, *84*, 1353–1366, doi:10.1175/BAMS-84-10-1353.

Meinvielle, M., and G. C. Johnson (2013), Decadal water-property trends in the California Undercurrent, with implications for ocean acidification, *J. Geophys. Res. Oceans*, *118*, 6687–6703, doi:10.1002/2013JC009299.
Olson, M. B., E. Lessard, C. H. J. Wong, and M. J. Bernhardt (2006), Copepod feeding selectivity on microplankton, including the toxigenic diatoms Pseudo-nitzschia spp., in the coastal Pacific Northwest, *Mar. Ecol. Prog. Ser.*, *326*, 207–220.
Olson, M. B., E. J. Lessard, W. P. Cochlan, and V. L. Trainer (2008), Intrinsic growth and microzooplankton grazing on toxigenic Pseudo-nitzschia spp. diatoms from the coastal northeast Pacific, *Limnol. Oceanogr. Methods*, *53*(4), 1352–1368.
Paulmier, A., I. Kriest, and A. Oschlies (2009), Stoichiometries of remineralisation and denitrification in global biogeochemical ocean models, *Biogeosciences*, *6*, 923–935.
Pelland, N. A., C. C. Eriksen, and C. M. Lee (2013), Subthermocline eddies over the Washington Continental Slope as Observed by Seagliders, 2003–09, *J. Phys. Oceanogr.*, *43*, 2025–2053, doi:10.1175/JPO-D-12-086.1.
Peterson, J. O., C. A. Morgan, W. T. Peterson, and E. Di Lorenzo (2013), Seasonal and interannual variation in the extent of hypoxia in the northern California Current from 1998–2012, *Limnol. Oceanogr. Methods*, *58*(6), 2279–2292, doi:10.4319/lo.2013.58.6.2279.
Pierce, S. D., R. L. Smith, P. M. Kosro, J. A. Barth, and C. D. Wilson (2000), Continuity of the poleward undercurrent along the eastern boundary of the mid-latitude north Pacific, *Deep Sea Res., Part II*, *47*(5–6), 811–829, doi:10.1016/S0967-0645(99)00128-9.
Pierce, S. D., J. A. Barth, R. K. Shearman, and A. Y. Erofeev (2012), Declining oxygen in the Northeast Pacific, *J. Phys. Oceanogr.*, *42*, 495–501, doi:10.1175/JPO-D-11-0170.1.
Reimers, C. E., H. Tuba Ozkan-Haller, P. Berg, A. Devol, K. McCann-Grosvenor, and R. D. Sanders (2012), Benthic oxygen consumption rates during hypoxic conditions on the Oregon continental shelf: Evaluation of the eddy correlation method, *J. Geophys. Res.*, *117*, C02021, doi:10.1029/2011JC007564.
Sarmiento, J. L., and N. Gruber (2006), *Ocean Biogeochemical Dynamics*, 528 p., Princeton Univ. Press, Princeton, N. J.
Shchepetkin, A. F., and J. C. McWilliams (2005), The regional oceanic modeling system (ROMS): A split-explicit, free-surface, topography-following-coordinate oceanic model, *Ocean Modell.*, *9*(4), 347–404.
Smith, S. L., Y. Yamanaka, M. Pahlow, and A. Oschlies (2009), Optimal uptake kinetics: Physiological acclimation explains the pattern of nitrate uptake by phytoplankton in the ocean, *Mar. Ecol. Prog. Ser.*, *384*, 1–12.
Stow, C. A., J. Jolliff, D. J. McGillicuddy, S. C. Doney, J. I. Allen, M. Friederichs, K. A. Rose, and P. Wallhead (2009), Skill assessment for coupled biological/physical models of marine systems, *J. Mar. Syst.*, *76*, 4–15, doi:10.1016/j.jmarsys.2008.03.011.
Thomson, R. E., and M. V. Krassovski (2010), Poleward reach of the California Undercurrent extension, *J. Geophys. Res.*, *115*, C09027, doi:10.1029/2010JC006280.
Trainer, V. L., B. M. Hickey, E. J. Lessard, W. P. Cochlan, C. G. Trick, M. L. Wells, A. MacFadyen and S. K. Moore (2009), Variability of Pseudo-nitzschia and domoic acid in the Juan de Fuca eddy region and its adjacent shelves, *Limnol. Oceanogr. Methods*, *54*(1), 289–308.
Tully, J. P. (1941), Surface non-tidal currents in the approaches to Juan de Fuca strait, *J. Fish. Res. Board Can.*, *5b*, 398–409, doi:10.1139/f40-041.
Venegas, R. M., P. T. Strub, E. Beier, R. Letelier, A. C. Thomas, T. Cowles, C. James, L. Soto-Mardones, and C. Cabrera (2008), Satellite-derived variability in chlorophyll, wind stress, sea surface height, and temperature in the northern California Current System, *J. Geophys. Res.*, *113*, C03015, doi:10.1029/2007JC004481.
Wanninkhof, R. (1992), Relationship between wind speed and gas exchange over the ocean, *J. Geophys. Res.*, *97*, 7373–7382, doi:10.1029/92JC00188.
Ward, B. B. (2008), Nitrification, in *Nitrogen in the Marine Environment*, edited by D. G. Capone et al., pp. 199–262, Elsevier, Amsterdam.
Ware, D. M., and R. E. Thomson (2005), Bottom-up ecosystem trophic dynamics determine fish production in the Northeast Pacific, *Science*, *308*, 1280–1284, doi:10.1126/science.1109049.
Wetz, M. S., B. Hales, and P. A. Wheeler (2008), Degradation of phytoplankton-derived organic matter: Implications for carbon and nitrogen biogeochemistry in coastal ecosystem, *Estuarine Coastal Shelf Sci.*, *77*, 422–432, doi:10.1016/j.ecss.2007.10.002.
Willmott, C. J. (1982), Some comments on the evaluation of model performance, *Bull. Am. Meteorol. Soc.*, *63*(11), 1309–1313, doi:10.1175/1520-0477(1982)063<1309:SCOTEO>2.0.CO;2.